Supplementary Materials for

Catenin α 1 mutations cause familial exudative vitreoretinopathy by overactivating Norrin/β-catenin signaling

Xianjun Zhu,[1,2,3] Mu Yang,[1,2] Peiquan Zhao,[4] Shujin Li,[1,2] Lin Zhang,[1] Lulin Huang,[1] Yi Huang,[1] Ping Fei,[4] Yeming Yang,[1] Shanshan Zhang,[1] Huijuan Xu,[1] Ye Yuan,[1] Xiang Zhang,[4] Xiong Zhu,[1] Shi Ma,[1] Fang Hao,[1] Periasamy Sundaresan,[5] Weiquan Zhu,[6] and Zhenglin Yang[1,2,3]

Correspondence should be addressed to:

Zhenglin Yang, Sichuan Provincial Key Laboratory for Human Disease Gene Study, Sichuan Provincial People's Hospital, University of Electronic Science and Technology of China,

32 The First Ring Road West 2, Chengdu, Sichuan, 610072, China

Email: zliny@yahoo.com

Phone: 86-28-87393375

Fax: 86-28-87393596

Contents

1. **Materials and Methods**
   - Patients and controls
   - DNA extract and whole-exome sequencing
   - Data analysis and mutation validation
   - Experimental animals

Immunohistochemistry and 5-ethynyl-2'-deoxyuridine (EdU) labeling of retinal endothelial cells
Hyaloid vessel imaging
Plasmids
Lentivirus-mediated siRNA knockdown and adenovirus-mediated overexpression
Cell culture and immunofluorescence staining
Isolation of mouse lung endothelial cells
Luciferase assays
Quantitative RT-PCR analysis
Co-immunoprecipitation and western blotting
Micro-CT scanning and data analysis
Electron microscopy
Image acquisition and statistical analysis

2. Supplemental Figures

Figure S1. Effect of wildtype or mutant *CTNNA1* on mRNA levels of endogenous β-catenin regulated genes in HRECs.
Figure S2. Effect of *CTNNA1* knockdown or *CTNNB1* overexpression on mRNA levels of endogenous β-catenin regulated genes in HRECs.
Figure S3. Knockdown of *CTNNA1* in HRECs increased cell proliferation.
Figure S4. Conditional knockout of *Ctnna1* in mouse endothelial cells caused severe vascularization defects.
Figure S5. Conditional knockout of *Ctnna1* in mouse endothelial cells caused severe delay in deep vessel development.

Figure S6. Heterozygous depletion of *Ctnna1* in mouse endothelial cells caused mild delay in deep vessel development.

Figure S7. Loss of *Ctnna1* in mouse ECs disrupts blood-retina barrier integrity.

Figure S8. Conditional knockout of *Ctnna1* in mouse endothelial cells caused abnormal expression of GFAP, Esm1 and Claudin-5.

Figure S9. DLL4 distribution in *Ctnna1* endothelial conditional knockout, *Lrp5* KO, *Fzd4* KO and *Ctnnb1* GOF Homo mice.

Figure S10. Loss of *Ctnna1* disrupts blood-brain barrier integrity.

Figure S11. Loss of *Ctnna1* in mouse ECs leads to leakage and activated astrocytes in the cerebellum.

Figure S12. Loss of *Ctnna1* in mouse ECs disrupts tight junction integrity in the cerebellum.

Figure S13. CDH5 regulates mice retinal vessel development and norrin/β-catenin signaling activity.

Figure S14. Disruption of adherens junctions and disorganization of F-ACTIN in isolated *Ctnna1*^{iECKO} and *Cdh5*^{iECKO} mouse lung endothelial cells.

Figure S15. Overexpression of CTNNA1 mutant proteins in *Ctnna1*^{iECKO} mouse lung endothelial cells failed to rescue the disruption of adherens junction and disorganization of F-ACTIN.

Figure S16. Overexpression of CTNNA1 mutant proteins in *Ctnna1*^{iECKO} mouse lung endothelial cells failed to inhibit β-catenin nuclear translocation.

Figure S17. Deletion of exon3 of *Ctnnb1* in mouse ECs resulted in accumulation of CTNNB1 protein in retinal ECs.

Figure S18. Gain of function of *Ctnnb1* allele in mice caused defect in deep vessel development.

Figure S19. An *LRP5* mutation in an Indian family with FEVR.

Figure S20. Mutation of *Lrp5 P847L* in mice caused delayed deep vessel development.

Figure S21. Genotyping of mouse models used in this study.

Figure S22. Crystal structure of human CTNNA1 (Protein Data Bank, PDB: 4IGG).

3. Supplemental Table S1-S12

Table S1 Family-34 3004 3016-filtered results.

Table S2. Clinical information of pedigree members in three families.

Table S3. Pathogenicity programs applied to mutations in *CTNNA1*.

Table S4. *Ctnna1*$^{flox/+}$, *Tie2-Cre* intercross F2 genotype.

Table S5. Survival time of *Ctnna1*$^{iECKO/iECKO}$ mice Tamoxifen induced from P1.

Table S6. Survival time of *Ctnna1*$^{iECKO/iECKO}$ mice Tamoxifen induced from P6

Table S7. *Ctnna1*$^{F72S/+}$ intercross F2 genotype.

Table S8. Primers for Sanger sequencing.

Table S9. Primers for mice genotyping

Table S10. Antibodies for Immunohistochemistry

Table S11. Primers for QPCR

Table S12. Antibodies for Western-blot

4. References

Materials and Methods

Patients and controls

Patients with FEVR and control individuals with no history of retinal degeneration were collected from Xinhua Hospital, Shanghai Jiaotong University, Sichuan Provincial People's Hospital, China and Aravind Eye Hospital, India. This research was carried out in accordance with the tenets of the Declaration of Helsinki and was approved by the ethical oversight committee of Sichuan Provincial People's Hospital, Xinhua Hospital, Shanghai Jiaotong University and Aravind Eye Hospital. Written informed consent was obtained from subjects who participated in this study or from the legal guardians of minors.

FEVR diagnosis was based on the examination of best-corrected visual acuity (BCVA), color vision, slit-lamp biomicroscopy, fundus photography, and by fundus fluorescein angiography (FFA), as previously described (1, 2). In total, 49 families with FEVR that did not carry mutations in genes known to be responsible for FEVR were collected.

DNA extract and whole-exome sequencing

Genomic DNA samples were extracted from peripheral blood leukocytes obtained from members of the 49 FEVR families and from1000 control individuals using a blood DNA extraction kit, according to the protocol provided by the manufacturer (TianGen). Exome sequencing was performed on DNA samples of the index patients. The DNA IlluminaTruSeqExome Capture System (62 Mb) was used to collect the protein-coding regions of the genomic DNA. The collected regions covered 20794 genes and 201121 exons in the Consensus Coding Sequence Region database (http://www.illumina.com/applications/sequencing/targetedresequencing.ilmn).

Data analysis and mutation validation

The high-quality sequencing reads were aligned to the human reference genome (NCBI build 37.1/ hg19) using SOAPaligner (soap2.21). Based on the SOAP alignment results, SOAPsnp v1.05 was used to assemble the consensus sequence and to call genotypes in target regions. Lists of sequence variants (SNPs and short Indels) were generated from this analysis. We filtered SOAPsnp results, using the following, previously described steps (3). SNP and Indel detection were performed only on exome regions and on flanking regions within size of 200 bp. Genomic variants were identified after reads were called, mapped and filtered against multiple databases. Mutation validation was then performed in patients and their relatives by Sanger sequencing, using an ABI 3730XL Genetic Analyzer with the primers listed in Table S8. Sequencing data were used to determine if the identified mutations co-segregated with the disease in these families and whether an identified mutation was absent in the 1000 ethnically matched controls.

Experimental animals

Mouse genotyping was carried out by PCR based methods using primers list in Table S9. Gel imaging data were presented in Figure S21.

A tamoxifen stock solution was prepared by dissolving 100 mg of tamoxifen salt (Sigma, St Louis, MO, USA) in 10 ml of ethanol. On the day of injection, a 1 mg/ml working solution was prepared by mixing the 10 mg/ml stock solution with corn oil (Sigma, St Louis, MO, USA). *Ctnna1*$^{iECKO/iECKO}$ mice and *Ctnnb1*$^{floxedExon3/floxedExon3}$ *Pdgfb-iCre* mice and littermate control mice of both genders were intraperitoneally injected with a daily dose of 25 mg/kg body weight of the 1 mg/ml tamoxifen solution on postnatal day 1-3 or 6-8 (6). Genomic DNA extracted from mouse-tails was amplified by PCR using primers listed in Table S9.

Immunohistochemistry and 5-ethynyl-2'-deoxyuridine (EdU) labeling of retinal endothelial cells

Retinal dissection was carried out as described previously (6), and whole-mounted retinas were preserved in 0.4% PFA (Sigma). Enucleated eyes were fixed with 4% PFA and embedded in Tissue-Tek optimal cutting temperature compound (Sakura Finetek). Before immunostaining, whole-mounted retinas and cryosections (12 μm, Leica CM1950) were rinsed in Phosphate buffered saline (PBS) (Sigma) three times (5 min/time) and blocked in PBS containing 5% fetal bovine serum (Invitrogen) and 0.2% Triton X-100 for 30 min at room temperature, followed by incubation with primary antibodies at 4°C overnight. Primary antibodies were diluted in blocking buffer at the following rates: Isolectin GS-IB_4 (1:100 dilution; I21411 ; Invitrogen), rat anti-mouse Ter119 (1:20 dilution; 553670; BD Bioscience), rat anti-mouse VE-Cadherin (1:100 dilution; 555289; BD Bioscience), goat anti-mouse Esm-1 (1:100 dilution; AF1999; R&D Systems), and rabbit anti-GFAP (1:100 dilution; 12389; Cell Signaling Technology), goat anti-mouse Vegf164 (1:100 dilution; AF-493-NA; R&D Systems), hamster anti-mouse Dll4 (1:100 dilution; 130802; Biolegend). The sections were then washed three times with PBS and labeled for 1–4 hours with Alexa Fluor™-488- or Alexa Fluor™-594-labelled goat anti-rat or anti-rabbit IgG or donkey anti-goat IgG secondary antibody (1:500 dilution; Invitrogen). Detailed primary and secondary antibodies were listed in Table S10.

To detect endothelial cell proliferation in retinas, 200 μg EdU (Invitrogen) per pup was injected intraperitoneally 3h before sacrificing. To detect proliferation of HRECs, 10μM EdU were pretreated for 3h. EdU-positive cells were subsequently stained with the Click-iT EdU Alexa Fluor-488 Imaging Kit (C10337; Invitrogen).

For Evans blue (Solarbio) leakage, 100μl of 2% Evans blue was intraperitoneal injected 24h prior to sacrifice.

Hyaloid vessel imaging

Hyaloid vessel isolation was performed as previously described (7). Eyes were removed on P9 mice and fixed with 4% PFA for 4 h. After removing the cornea and iris, eyes were steeped in 5% (w/v) gelatin (Invitrogen) at 37°C overnight. The hyaloid vessel was dissected on ice, then melted and dried on a glass slide before staining with DAPI.

Plasmids

Wild type CTNNA1 or CDH5 coding sequence was subcloned into a mammalian expression vector with N-terminal FLAG tag pCDNA3.1 vector. Norrin, FZD4 and LRP5 were cloned in pCMV6 and pRK5 vectors. *CTNNA1-F72S*, *CTNNA1-R376Cfs*27*, *CTNNA1- P893L* and *LRP5-P848L* were generated by site-directed mutagenesis. pGL4.1 (Renilla luciferase) was from Promega Biosciences Inc.

Lentivirus-mediated siRNA knockdown and adenovirus-mediated overexpression

HRECs at passages 3-7 and HEK293STF were transduced with a lentivirus carrying shRNA targeting *CTNNA1* (5'-CACCTCAGAGATGGACAACTA-3', Genechem), *CTNND1 (5'*-CAGCCAGAGGTGGTTCGGATATACA-*3')* and *CDH5* (5'-TGGATTACGACTTCCTTAA-3') or with negative-control shRNA (5'-TTCTCCGAACGTGTCACGT-3'), according to the manufacture's instruction. HEK293 STF cells that stably express the shRNA were selected with puromycin. The overexpression of control and CTNNA1-F72S and CTNNA1-P893L in HRECs were mediated by adenovirus (Hanbio). The efficiency of knockdown or overexpression

was assessed by immunofluorescence staining or western blotting 72 h after transduction.

Cell culture and immunofluorescence staining

HEK293 STF cells were purchased from ATCC (American Type Culture Collection, CRL-3249™) and maintained in Dulbecco's modified Eagle's medium (DMEM) supplemented with 10% fetal calf serum (FCS), 100 mg/ml penicillin, and 100 mg/ml streptomycin at 37°C in a 5% CO_2 atmosphere. HRECs (primary human retinal microvascular endothelial cells, obtained from Cell Systems, ACBRI 181) were cultured in EGM™-2 media (Lonza) at 37°C in a 5% CO_2 incubator. To observe nuclear translocation of β-catenin, Norrin (1.25 μg/mL) were pretreated for 15 min to activate Norrin/β-catenin signaling.

For immunofluorescence, HRECs were seeded on 5μg/ml human fibronectin protein (Thermo Fisher Scientific) coated slices in 24-well plates (Corning) before virus infection. After being fixed in 4% PFA in PBS at room temperature for 20 min, slices underwent the above-mentioned rinse and blocking procedure, followed by incubation with primary antibodies at 4°C overnight and with secondary antibodies for 1 h at room temperature. Detailed primary and secondary antibodies were listed in Table S10.

Isolation of mouse lung endothelial cells

Primary mouse lung ECs were isolated as previously described using CD31 and CD102 dynabeads (Invitrogen) (8).

Luciferase assays

The luciferase assays were performed as previously described (9). To investigate the luciferase activity upon knockdown of *CTNNA1*, cells were cotransfected with plasmids mix (including 100 ng *NORRIN*, 100 ng *LRP5*, 100 ng *FZD4* and 200 ng

pGL4.1) using Lipofectamine 3000 Transfection Reagent (Thermo Fisher Scientific) at 70% confluence. After incubation for 48 h, firefly and renilla luciferase activities were measured using a Dual-Luciferase Reporter Assay System (TransGen Biotec). Reporter activity was calculated in terms of the relative luciferase units (RLU) of the firefly/renilla activity in each well compared with that of HEK293 STF cells transfected with control virus. The luciferase assays were performed as a minimum four times.

To investigate luciferase activity upon overexpression of WT *CTNNA1* and mutant alleles of *CTNNA1,* cells were cotransfected with 100 ng of the appropriate *CTNNA1* allele and plasmids mix. The value of the cells transfected with WT plasmid was set to1.

Quantitative RT-PCR analysis

Total RNA was extracted from HRECs with RNeasy Mini kits (QIAGEN), and 1μg total RNA was reverse transcribed with EasyScript One-Step RT-PCR SuperMix (TransGen Biotech) following the manufacturer's instructions. cDNA was amplified using TransStart Tip Green qPCR SuperMix (TransGen Biotech) in a 7500 Fast Real-Time PCR System (Applied Biosystems). Primers were listed in Table S11.

Co-immunoprecipitation and western blotting

Co-immunoprecipitation assays were performed as previously described (10). The interaction of WT and mutant CTNNA1 with endogenous CTNNB1 and VE-Cadherin was investigated. Briefly, Flag-labeled wild type CTNNA1 or mutant CTNNA1 was overexpressed in HRECs mediated by adenovirus. Cells were washed with cold PBS and lysed with cold lysis buffer containing 250mM NaCl, 50mM Tris-HCL, 1% NP-40, 10% glycerol supplemented with phosphatase and protease inhibitors (Sigma-Aldrich). Cell lysates were centrifuged at 13,000 × g for 15 min,

and the soluble supernatants were pre-cleaned with protein A/G sepharose beads (Santa Cruz Biotechnology) at 4°C for 1 h. The pre-cleaned lysates were then centrifuged at 1000× g for 3 min, and the supernatants were collected into new tubes. The supernatants were further incubated with anti-FLAG M2 agarose (Sigma-Aldrich) at 4°C overnight. After incubation, protein-bound beads were washed 4 times with cold lysis buffer, resuspended in 6× loading buffer (TransGen Biotech) and heated at 70°C for 10 min. Beads were precipitated by centrifugation at 1000× g for 3 min, and the supernatants were subjected to western blotting. The interaction between Flag-CTNNA1 and endogenous CTNNB1 or VE-Cadherin was assessed following staining with primary antibodies and HRP-linked secondary antibodies.

Micro-CT scanning and data analysis

Tissue specimens were stained with 5% Lugol's solution and scanned with Zeiss Xradia 520 Versa X-ray Microscopes (Carl Zeiss Co. Ltd., Shanghai, China). Specimens were mounted on the holder with a centrifuge tube as an adapter and rotated horizontally by 360 degrees, pausing at discrete angles to collect 2D projection images, which were then combined to produce a 3D reconstruction of the specimen’s volume dataset. The scanning energy was 90kV/8 W. The scanning resolution was between 3 and 4μm, depending on the size of the region of interest (ROIs). Low-resolution scanning was performed for whole-brain scanning, and fine-resolution scanning was carried out for cerebellum scanning. Three-dimensional reconstruction and vessel rendering were performed using the software ORS Visual.

Electron microscopy

The samples were prefixed with a mixed solution of 4% paraformaldehyde and 2.5% glutaraldehyde, then the tissue was postfixed in 1% osmium tetroxide and dehydrated step by step with acetone, embedded with Epon 812. The semithin

sections were stained with methylene blue and ultrathin sections were cut with diamond knife, stained with uranyl acetate and lead citrate. Sections were examined using JEM-1400 Flash Transmission Electron Microscope.

Image acquisition and statistical analysis

Confocal images were obtained with 10×, 20× or 40× objective lens using a Laser Scanning Microscope 800 (LSM 800, Zeiss, Jena, Germany). The Zen 2.1 software was used for the measurement of cell junction proteins, the 'Spline Contour2' tool were used to calculate 'Intensity Mean Value' of junctional regions between two adjacent cells. For vessel area measurement of flat-mounted retinas, the software "Angiotool" was used as indicated (11). Vessel progression was analyzed by measuring the distance from the optic nerve to the vascular front using Zen 2.1 software. The 'Vessels percentage area' data was calculated using 'Angiotool' software as vessel density (%). However, the vessel structure of *Ctnna1*$^{iECKO/iECKO}$ retinas after P6 could not be detected by 'Angiotool' due to the increase of vessel density and alteration of vessel structures, thus we determine the vessel density by calculating 'Intensity Mean Value' of IB4 signal using Zen 2.1 software. EdU+ endothelial cells were counted within a 20×objective lens snap picture, the vessel area measurement was calculated by total area multiplied by 'vessel density' demonstrated above. Vessel leakage was determined by the ratio of Ter119 leakage area to total retinal area, area was measured using Zen 2.1 software. Western blotting signals were detected by Image Quant LAS 500 (GE Life Sciences), and the software ImageJ was used to quantify the detected signals. Crystal structures were analysed and generated using the PyMol software.

Statistical analysis was performed with GraphPad Prism 6.0. Comparison between two experimental groups were analyzed with unpaired Student's t-tests with

Welch's correction, while multiple comparisons between more than two experimental groups were assessed with one-way or two-way ANOVA with Tukey's or Dunnett's multiple comparisons test to assess statistical significance with a 95% confidence interval. $p \leq 0.05$ was considered to be statistically significant.

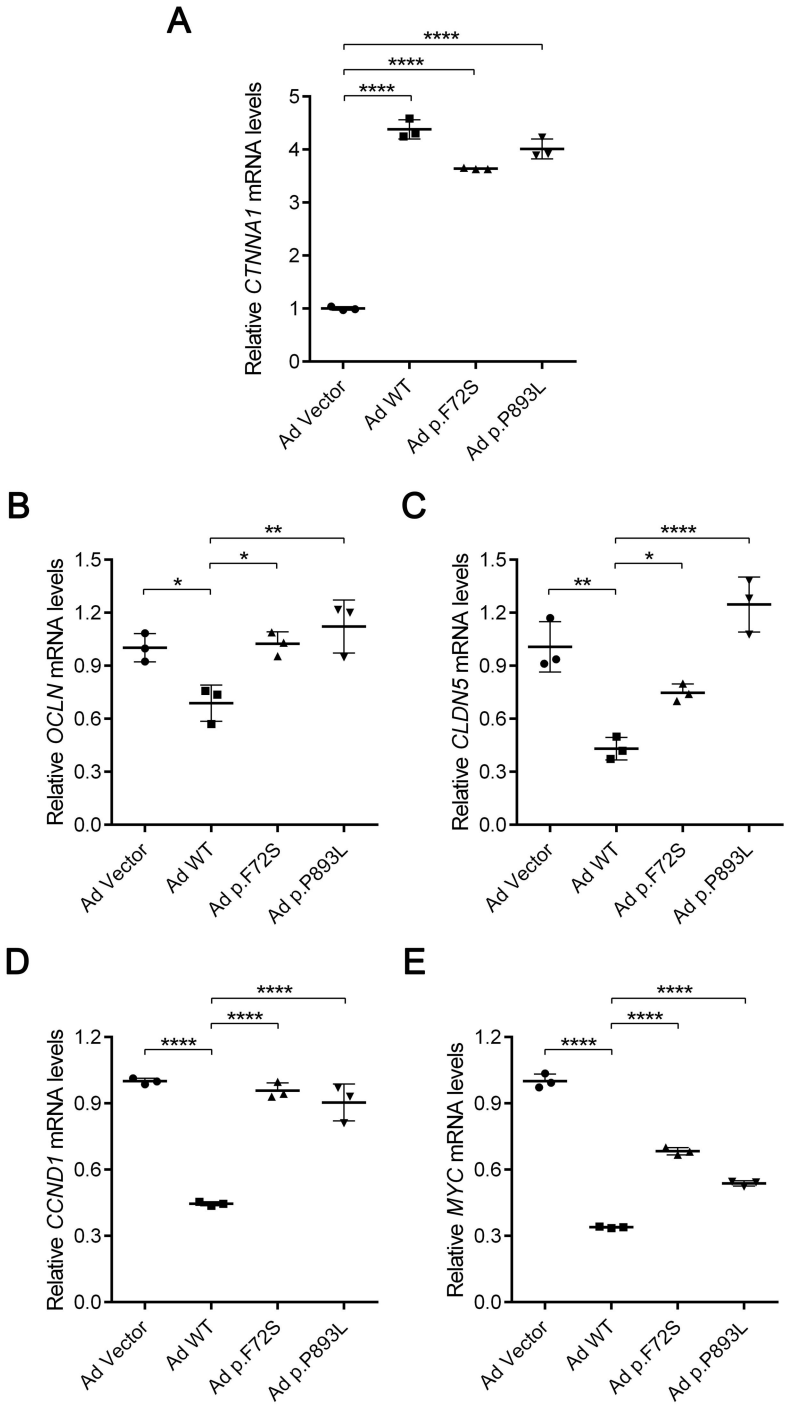

1

2 **Figure S1. Effect of wildtype or mutant *CTNNA1* on mRNA levels of endogenous**

3 **β-catenin regulated genes in HRECs.** (A-E) (C) Quantification of qPCR analysis

4 showing relative mRNA levels of *CTNNA1, OCLN, CLDN5, CCND1* and *MYC* in

5 HRECs overexpressed with Vector, wildtype, p.F72S or p.P893L form of CTNNA1.

Error bars, SD. *p*-values from multiple comparisons in one-way ANOVA with Dunnett's multiple comparisons test (n=3), * $p<0.05$, ** $p<0.01$, **** $p<0.0001$. Experiments were performed at least three times independently.

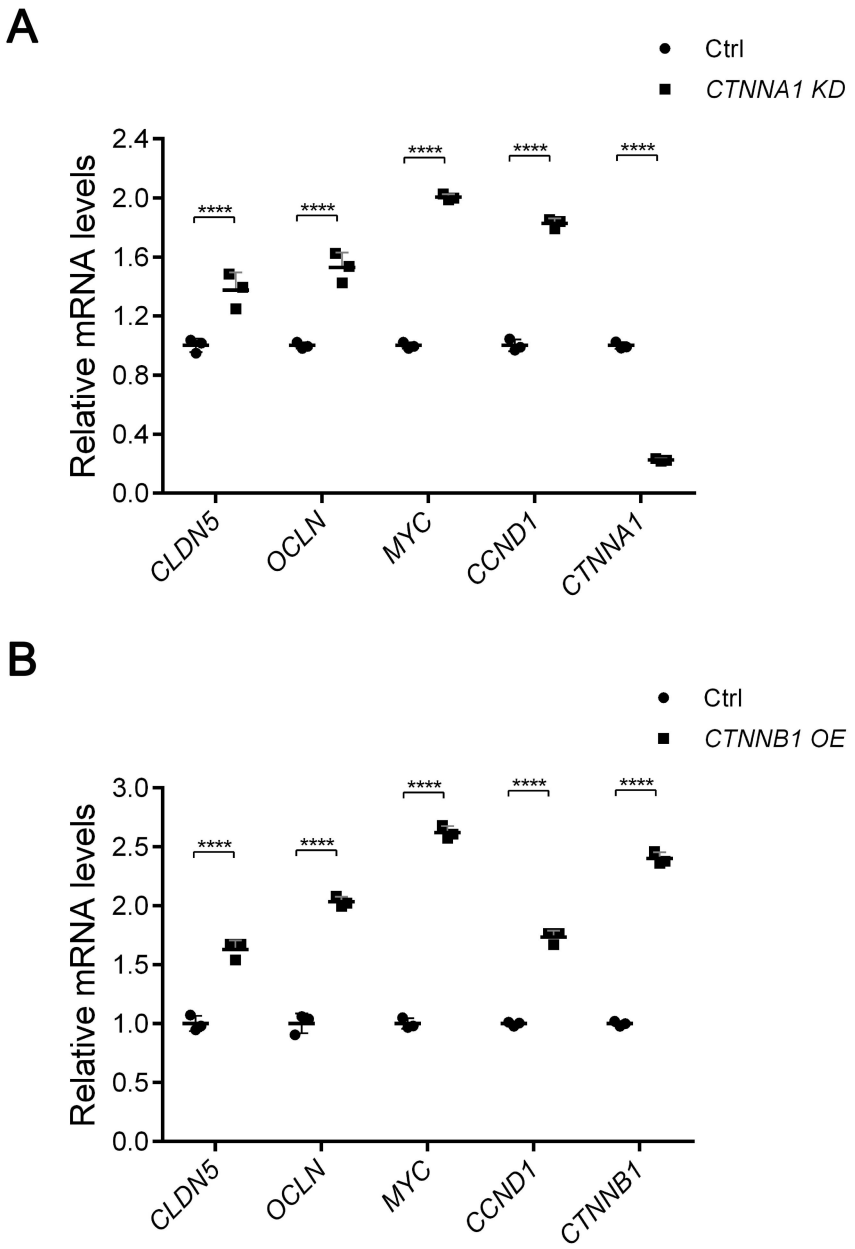

Figure S2. Effect of *CTNNA1* knockdown or *CTNNB1* overexpression on mRNA levels of endogenous β-catenin regulated genes in HRECs. (A) Quantification of qPCR analysis showing relative mRNA levels of *CTNNA1, OCLN, CLDN5, CCND1* and *MYC* in *CTNNA1* KD HRECs. Error bars, SD. *p*-values from multiple comparisons in two-way ANOVA with Sidak's multiple comparisons test (n=3), **** $p<0.0001$. (B) Quantification of qPCR analysis showing relative mRNA levels of *CTNNB1, OCLN, CLDN5, CCND1* and *MYC* in HRECs overexpressed with *CTNNB1*. Error bars, SD. *p*-values from multiple comparisons in two-way ANOVA with

Sidak's multiple comparisons test (n=3), **** $p<0.0001$. Experiments were performed at least three times independently.

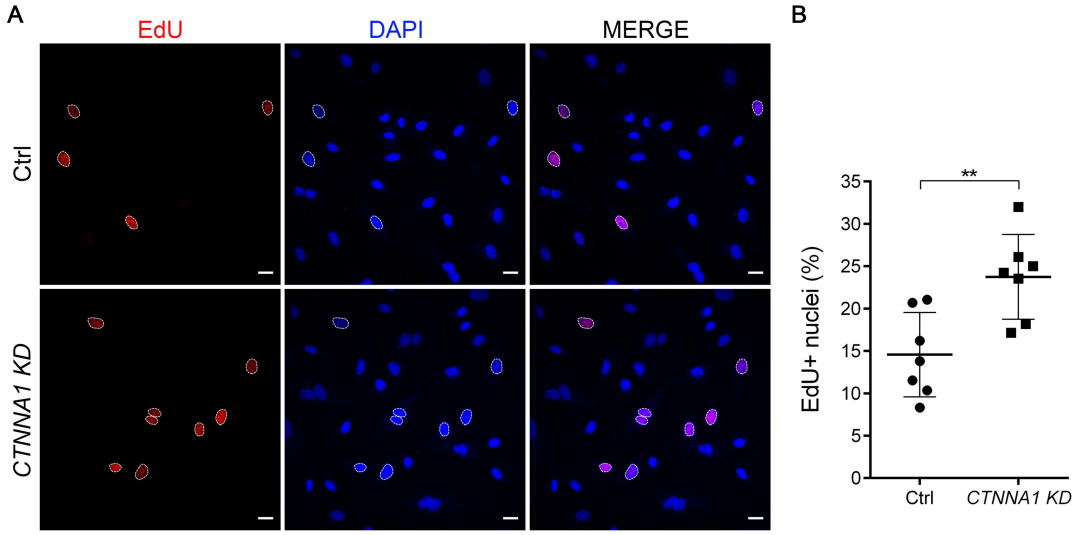

Figure S3. Knockdown of *CTNNA1* in HRECs increased cell proliferation. (A) Representative confocal images of HRECs transfected with control or *CTNNA1* shRNA co-stained with DAPI (blue) and EdU (red). Scale bars, 25μm. (D) Quantification of percentage of EdU+ nuclei (%). Error bars, SD. Student's t-test (n=7), ** $p<0.01$. Experiments were performed at least three times independently.

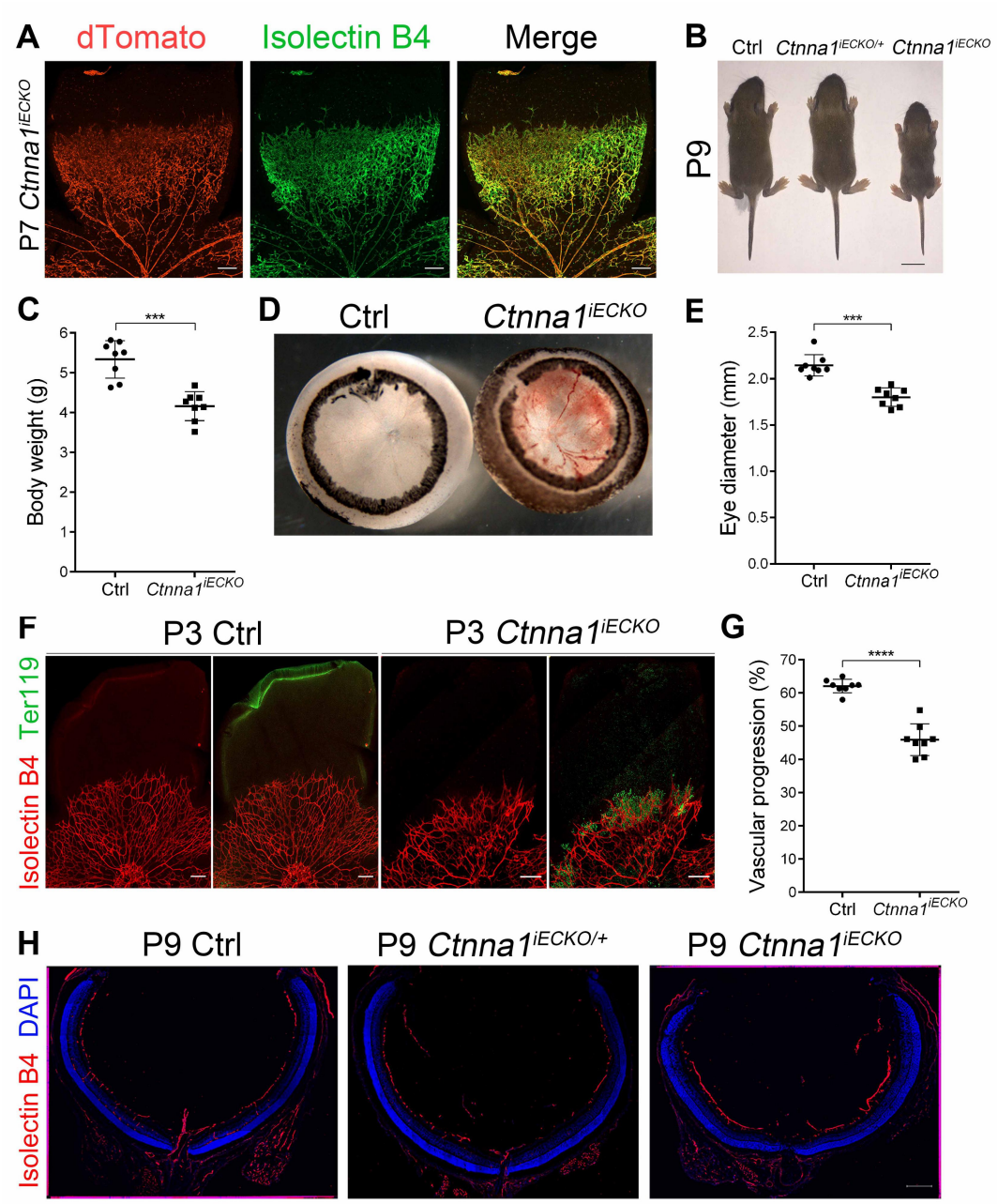

Figure S4. Conditional knockout of *Ctnna1* in mouse endothelial cells caused severe vascularization defects. (A) P7 *Ctnna1*$^{iECKO/iECKO}$ (hereafter named *Ctnna1*^{iECKO}) ROSA-tdTomato mice retinas were stained with Isolectin B4 (IB4, green). The fluorescent tdTomato signal co-localized with IB4, indicating that recombinant CRE was specifically expressed in endothelial cells. Scale bars, 250μm. (B) Body size of P9 control mice (hereafter named Ctrl), *Ctnna1*$^{iECKO/+}$ and *Ctnna1*^{iECKO} mice. Scale bars, 1cm. (C) Quantification of body weight at P9. Error

bars, SD. Student's t-test (n=8). *** $p<0.001$. (D) Bright-field image of eyeballs of Ctrl and *Ctnna1*^{iECKO} mice at P9, showing hemorrhage and enlargement of blood vessels in the eye. (E) Quantification of eye diameter at P9. Error bars, SD. Student's t-test (n=8). *** $p<0.001$. (F) Ter119 (green) and IB4 (red) staining of P3 retinas of Ctrl and *Ctnna1*^{iECKO} mice retina wholemount, showing delayed outgrowth and erythrocyte leakage. Scale bars, 250μm. (G) Quantification of vascular progression at P3. Error bars, SD. Student's t-test (n=8). **** $p<0.0001$. (H) Frozen section of Ctrl, *Ctnna1*$^{iECKO/+}$ and *Ctnna1*^{iECKO} mice retinas were stained with IB4 (red) and DAPI (blue). Scale bars, 250μm. Experiments were performed at least three times independently.

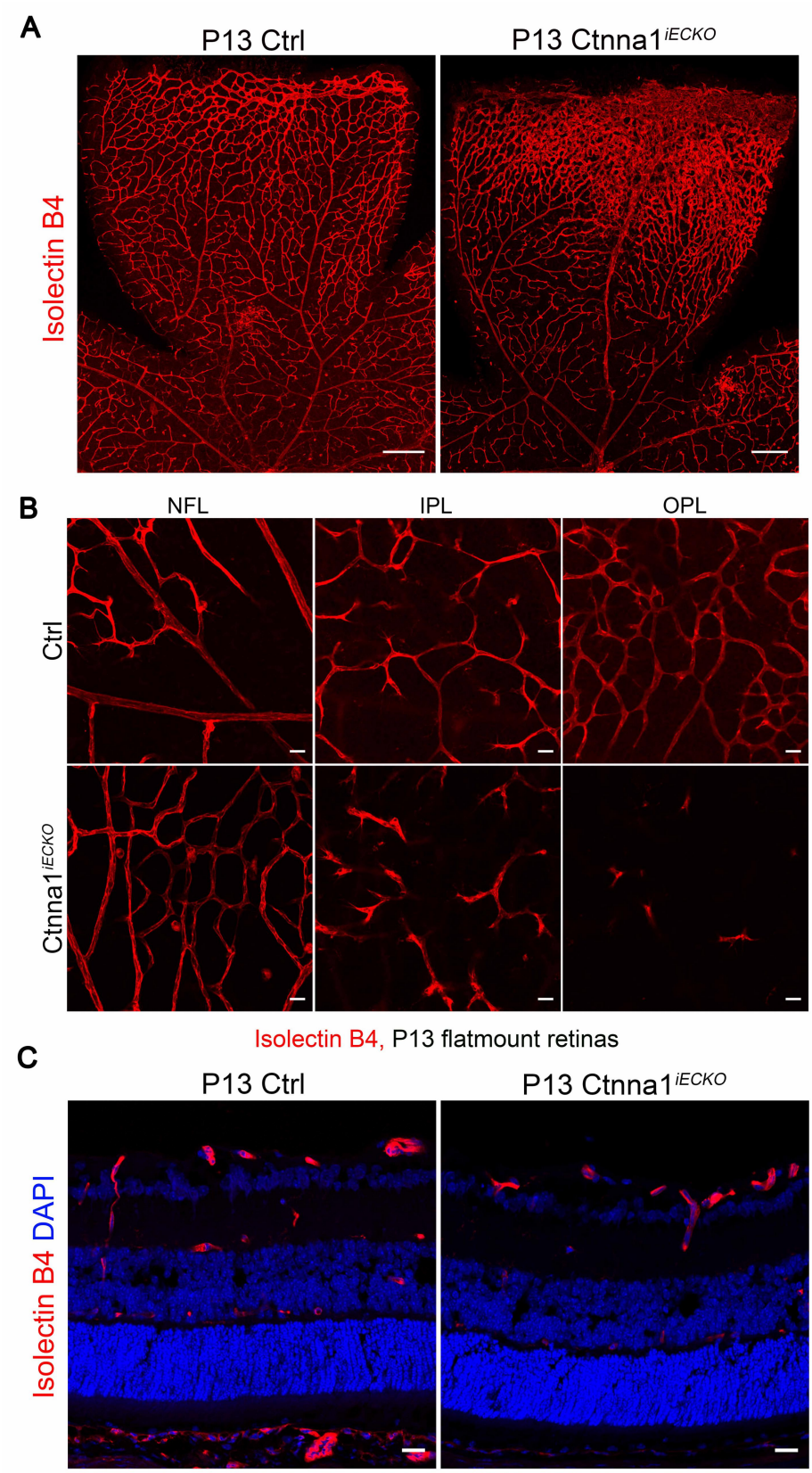

1

2 **Figure S5. Conditional knockout of *Ctnna1* in mouse endothelial cells caused**

3 **severe delay in deep vessel development.** (A) IB4 (red) immunofluorescence of P13

(tamoxifen induced from P6) control and *Ctnna1*^{iECKO} mice retina flat mounts showing abnormal enlargement of vessel at the peripheral area of the retina. Scale bars, 200μm. (B) Confocal projections of IB4 (red) stained NFL, IPL and OPL of P13 control and *Ctnna1*^{iECKO} mice retina flat mounts. Scale bars, 20μm. (C) Retinal frozen sections of P13 Ctrl and *Ctnna1*^{iECKO} mice were co-stained with IB4 (red) and DAPI (blue). Scale bars, 20μm. Experiments were performed at least three times independently.

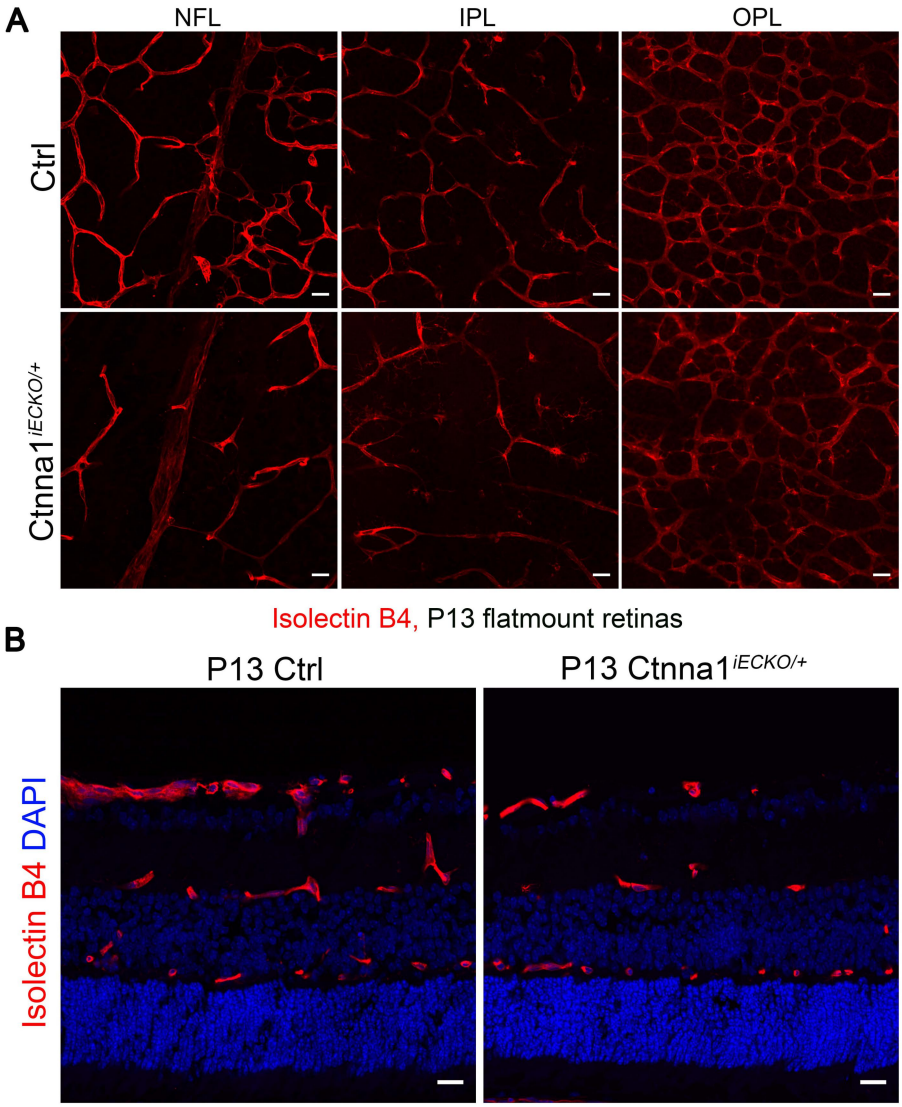

1

2 **Figure S6. Heterozygous depletion of *Ctnna1* in mouse endothelial cells caused**

3 **mild delay in deep vessel development.** (A) Confocal projections of IB4 (red)

4 stained NFL, IPL and OPL of P13 control and *Ctnna1*$^{iECKO/+}$ mice retina flat mounts.

5 Scale bars, 20μm. (B) Retinal frozen sections of P13 Ctrl and *Ctnna1*$^{iECKO/+}$ mice co-

6 stained with IB4 (red) and DAPI (blue). Scale bars, 20μm. Experiments were

7 performed at least three times independently.

8

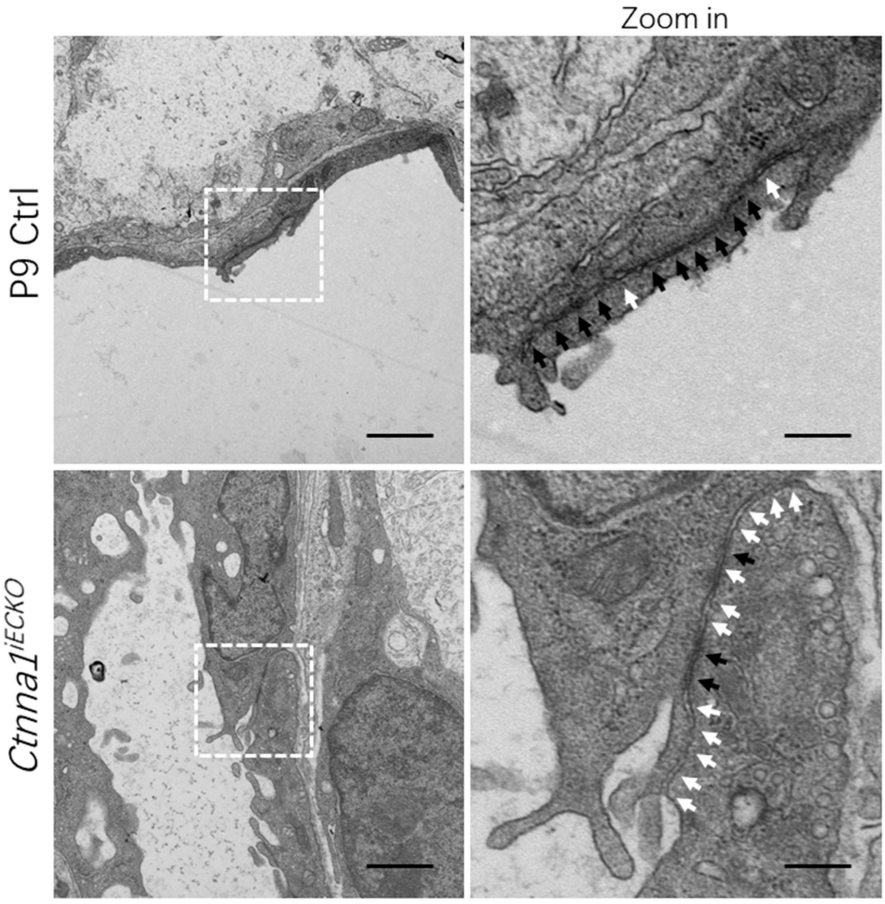

Figure S7. Loss of *Ctnna1* in mouse ECs disrupts blood-retina barrier integrity. Representative overview (left panels) and high-magnification (right panels) electron microscope images of P9 control and *Ctnna1*^{iECKO} mice retina. Dotted boxes indicate magnified areas. Black arrows or white arrows indicate continuous or discontinuous junctions between two adjacent ECs. Scale bars, 1μm (left panels) and 250nm (right panels). Experiments were performed at least three times independently.

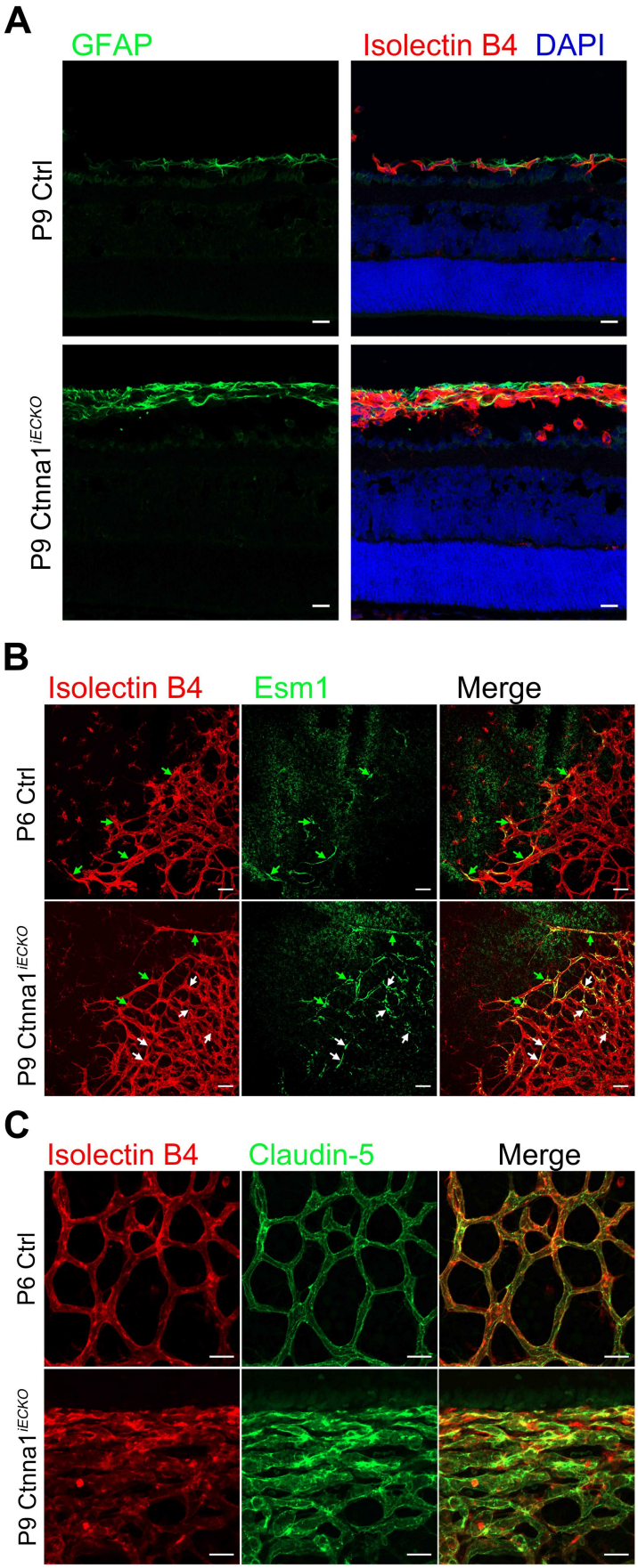
A
GFAP
Isolectin B4
DAPI
P9 Ctrl
P9 Ctnna1iECKO
B
Isolectin B4
Esm1
Merge
P6 Ctrl
P9 Ctnna1iECKO
C
Isolectin B4
Claudin-5
Merge
P6 Ctrl
P9 Ctnna1iECKO

1

Figure S8. Conditional knockout of *Ctnna1* in mouse endothelial cells caused abnormal expression of GFAP, Esm1 and Claudin-5. (A) Frozen sections of P9 retinas of Ctrl and *Ctnna1*^{iECKO} mice retinas were co-stained with GFAP (green), IB4 (red) and DAPI (blue). Increased GFAP expression was observed, indicative of retinal stress. Scale bars, 25μm. (B) Tip cell marker Esm1 (green) and IB4 (red) were stained in P6 *Ctnna1*^{iECKO} mice retina wholemount. Esm1 was expressed in the angiogenic front of Ctrl and *Ctnna1*^{iECKO} mice retinas, whereas the stalk cells in the remodeling plexus of *Ctnna1*^{iECKO} mice retinas abnormally expressed Esm1. Scale bars, 25μm. Green arrows denote normal tip cell expression of Esm1. White arrows denote abnormal expression of stalk cell Esm1. (C) β-catenin regulated tight junction protein Claudin-5 (green) and IB4 (red) were stained in P6 *Ctnna1*^{iECKO} mice retina wholemount showing increased and abnormal distribution of Claudin-5 signal. Scale bars, 25μm. Experiments were performed at least three times independently.

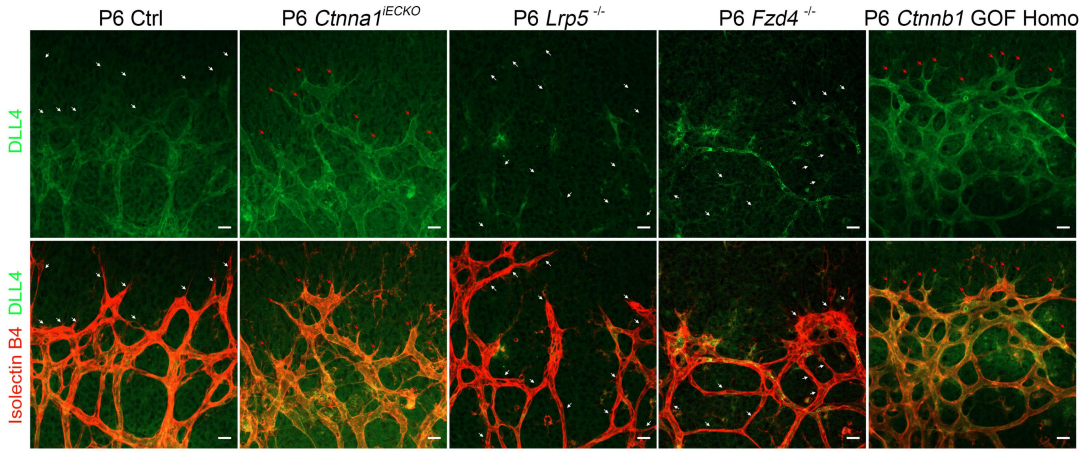

Figure S9. DLL4 distribution in *Ctnna1* endothelial conditional knockout, *Lrp5* KO, *Fzd4* KO and *Ctnnb1* GOF Homo mice. In retinas of P6 control littermates, DLL4 (green) was restricted to the stalk cells of retina vessels. However, DLL4 was abnormally expressed in both the tip cells and stalk cells in P6 *Ctnna1*^{iECKO} and *Ctnnb1* GOF Homo retinas, whereas diminished in the vascular of both P6 *Lrp5* and *Fzd4* KO mice retinas. White arrows denote the absence of DLL4 in the vascular cells; red arrows denote abnormal DLL4 expression in tip cells. Scale bar, 25μm. Experiments were performed at least three times independently.

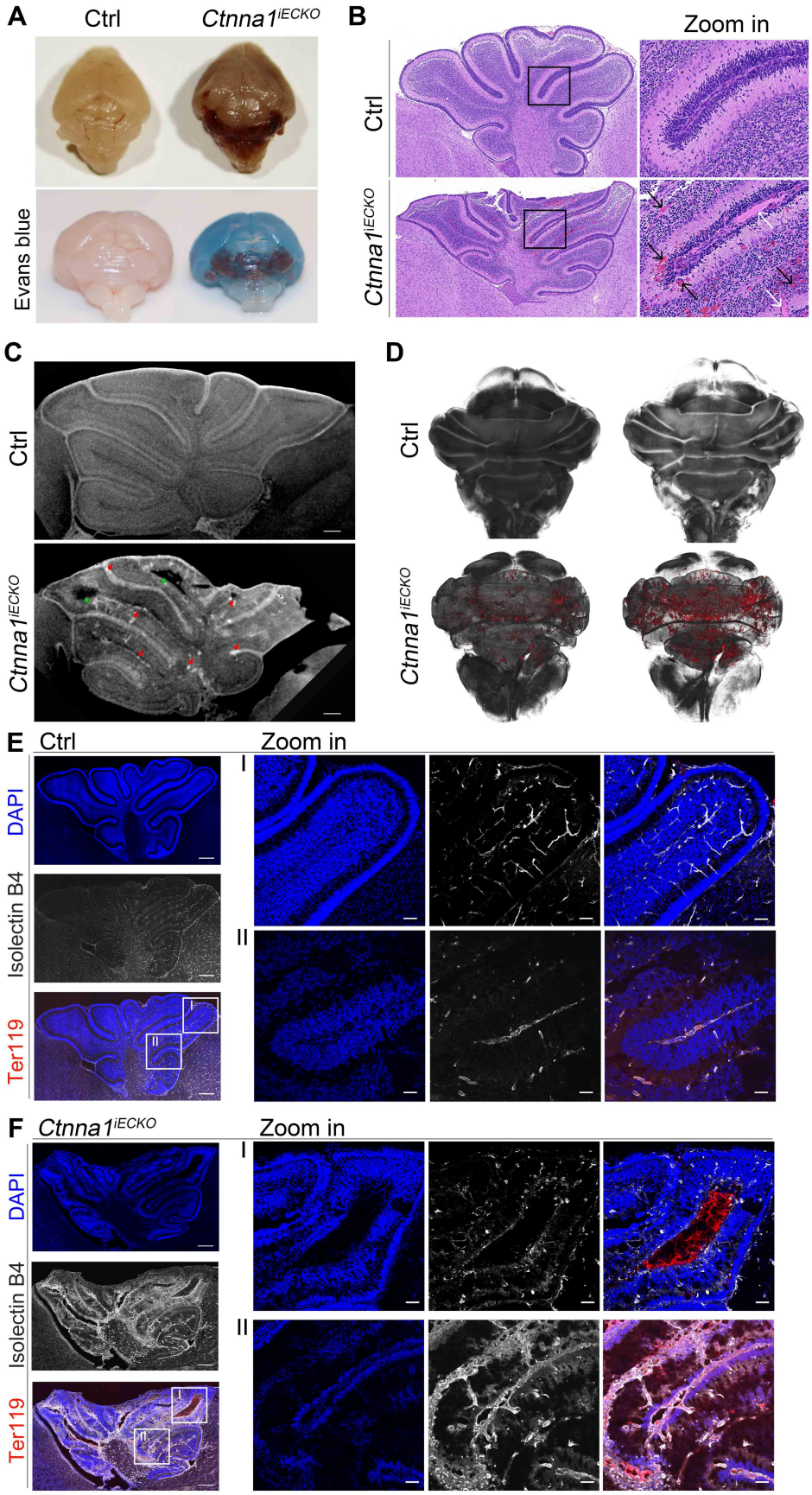
A
Ctrl
Ctnna1iECKO
Evans blue
B
Zoom in
Ctrl
Ctnna1iECKO
C
Ctrl
Ctnna1iECKO
D
Ctrl
Ctnna1iECKO
E
Ctrl
Zoom in
DAPI
Isolectin B4
Ter119
I
II
F
Ctnna1iECKO
Zoom in
DAPI
Isolectin B4
Ter119
I
II

1

Figure S10. Loss of *Ctnna1* disrupts blood-brain barrier (BBB) integrity. (A) Extensive leakage of Evans blue was observed in the whole brains of P9 *Ctnna1*^{iECKO} mice after intraperitoneal injection and their cerebellum appeared intensively red. (B) Hematoxylin and eosin stained, sagittal sections of P9 control and *Ctnna1*^{iECKO} cerebellum. White arrows indicate abnormal proliferation and black arrows, enlarged vascular vessels in the mutant. (C) Sagittal projections of control (top) and *Ctnna1*^{iECKO} (lower) cerebellum generated by X-ray micro-computed tomography (micro-CT). High-intensity (red arrows) and low-intensity (green arrows) areas are shown. Scale bars, 250μm. (D) Three-dimensional images of control (top) *Ctnna1*^{iECKO} (lower) cerebellum. Red structures indicate enlarged blood vessels. (E, F) Ter119 and IB4 staining of P9 Ctrl and *Ctnna1*^{iECKO} cerebellum. Scale bars, 250μm. White boxes show magnified regions, detailed on right, scale bars, 25μm. The magnified images showed extensive leakage of erythrocytes and blood vessel enlargement, as well as edema-like cavities, in *Ctnna1*^{iECKO} cerebellum. Experiments were performed at least three times independently.

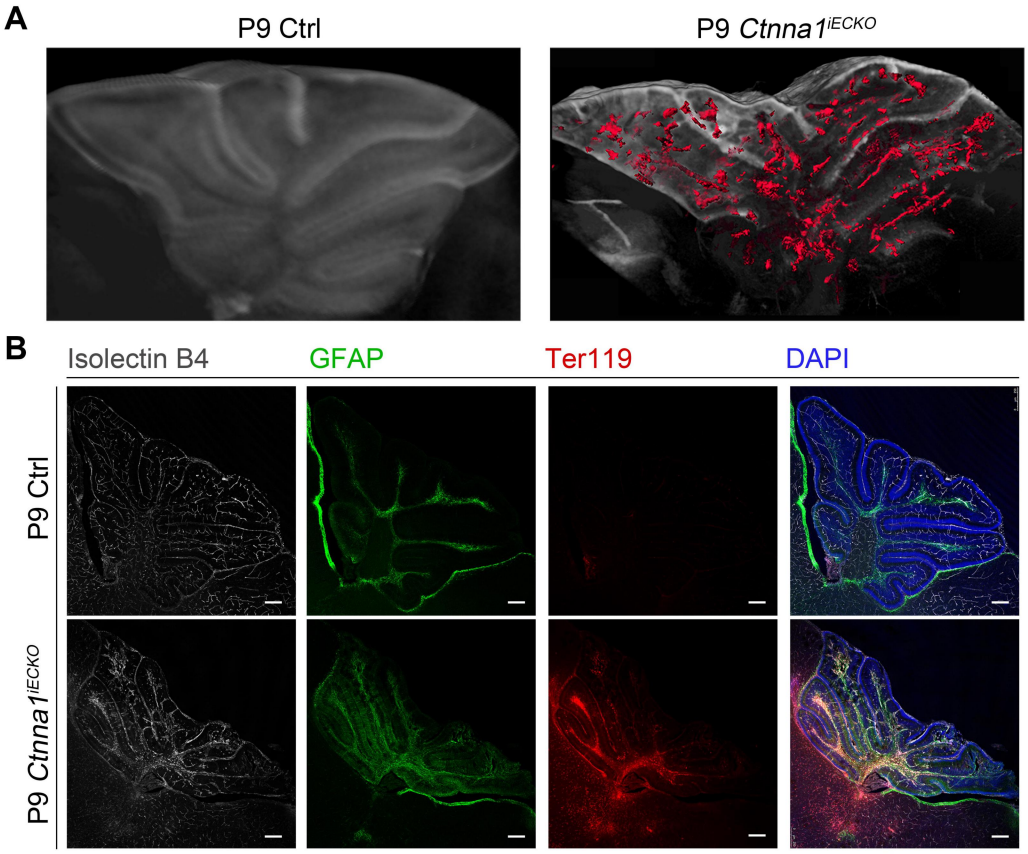

Figure S11. Loss of *Ctnna1* in mouse ECs leads to leakage in the cerebellum. (A) The 3D sagittal projection of Ctrl (left) and *Ctnna1*^{iECKO} (right) cerebellum. Red structures indicate enlarged blood vessels. (B) Quadruple staining with IB4 (white), GFAP (green), Ter119 (red), and DAPI (blue) on frozen sections of P9 control and *Ctnna1*^{iECKO} cerebellum. Scale bars, 500μm. Experiments were performed at least three times independently.

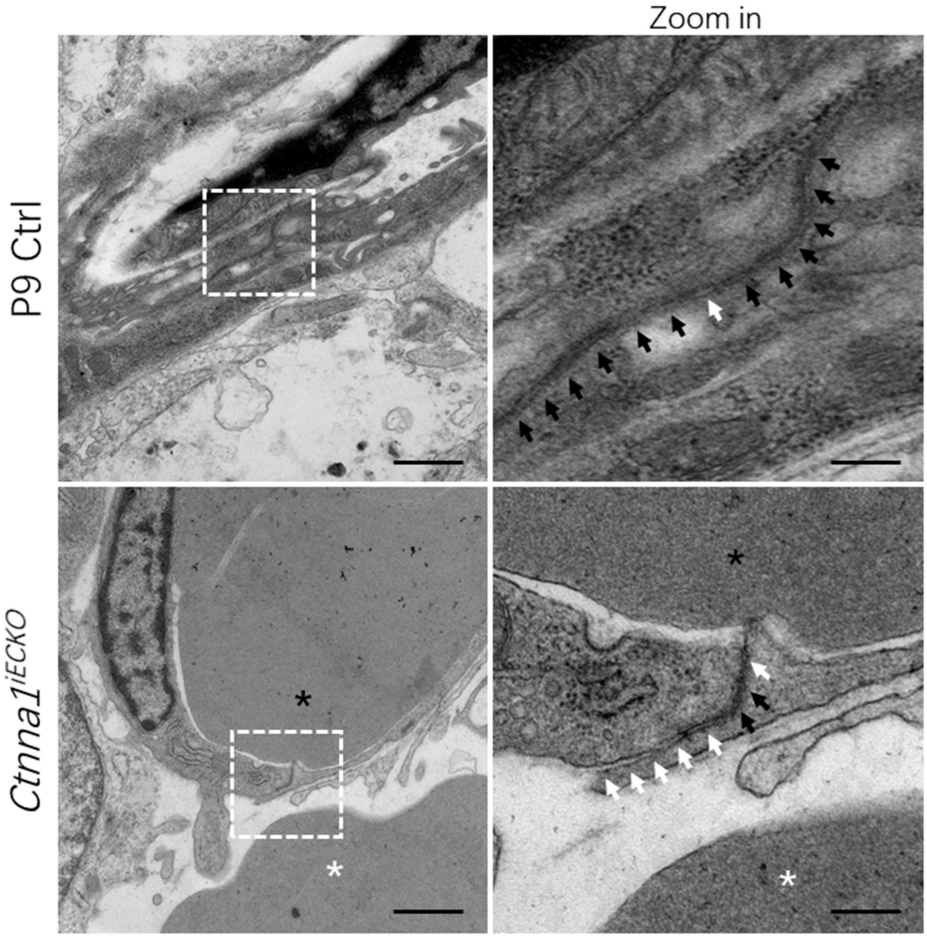

Figure S12. Loss of *Ctnna1* in mouse ECs disrupts blood-brain barrier integrity. Representative overview (left panels) and high-magnification (right panels) electron microscope images of P9 control and *Ctnna1*^{iECKO} mice cerebellum. Dotted boxes indicate magnified areas. Black * or white * indicate erythrocytes in or out of vessels, respectively. Black arrows or white arrows indicate continuous or discontinuous junctions between two adjacent ECs. Scale bars, 1μm (left panels) and 250nm (right panels). Experiments were performed at least three times independently.

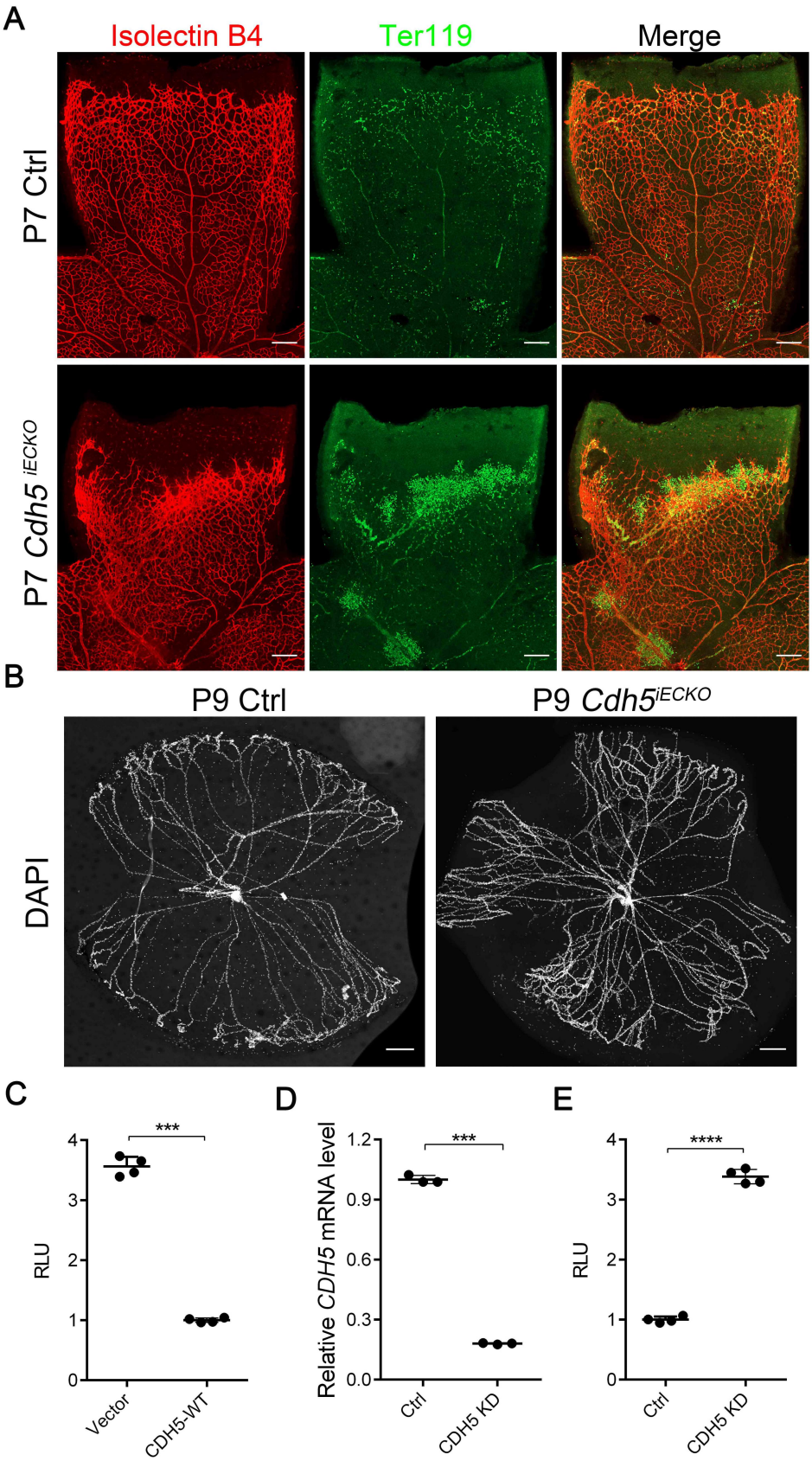
A
Isolectin B4
Ter119
Merge
P7 Ctrl
P7 Cdh5 iECKO
B
P9 Ctrl
P9 Cdh5iECKO
DAPI
C
D
E
RLU
Relative CDH5 mRNA level
Vector
CDH5-WT
Ctrl
CDH5 KD
***
****

1

Figure S13. CDH5 regulates mouse retinal and hyaloid vessel development and norrin/β-catenin signaling activity. (A) Anti-Ter119 (green) and IB4 (red) immunofluorescence of P7 Ctrl and *Cdh5*^{iECKO} mice retinas. Scale bars, 200μm. (B) DAPI staining of hyaloid vessels in the eyes of control and *Cdh5*^{iECKO} mice, showing that hyaloid vessel regression was significantly delayed. Scale bar, 200μm. (C) Results of luciferase reporter assay in HEK293 STF cells. Cells were transfected with plasmids containing *CDH5-WT* or an empty vector (pCDNA3.1). Plasmids were co-transfected with *LRP5, FZD4, NDP* and *Renillareniformis* (PGL4.1). The activity of WT protein was normalized as 1. Error bars, SD (standard deviation). *p*-values, Student's t-test (n=4); *** $p<0.001$. (D) QPCR analysis demonstrated efficient shRNA-mediated knockdown of *CDH5* in HEK 293STF cells. Error bars, SD. *p*-values, Student's t-test (n=3); *** $p<0.001$. (E) ShRNA-mediated knockdown of *CDH5* in the 293STF cell line led to elevated luciferase activity. Error bars, SD. *p*-values, Student's t-test (n=4); **** $p<0.0001$. Experiments were performed at least three times independently.

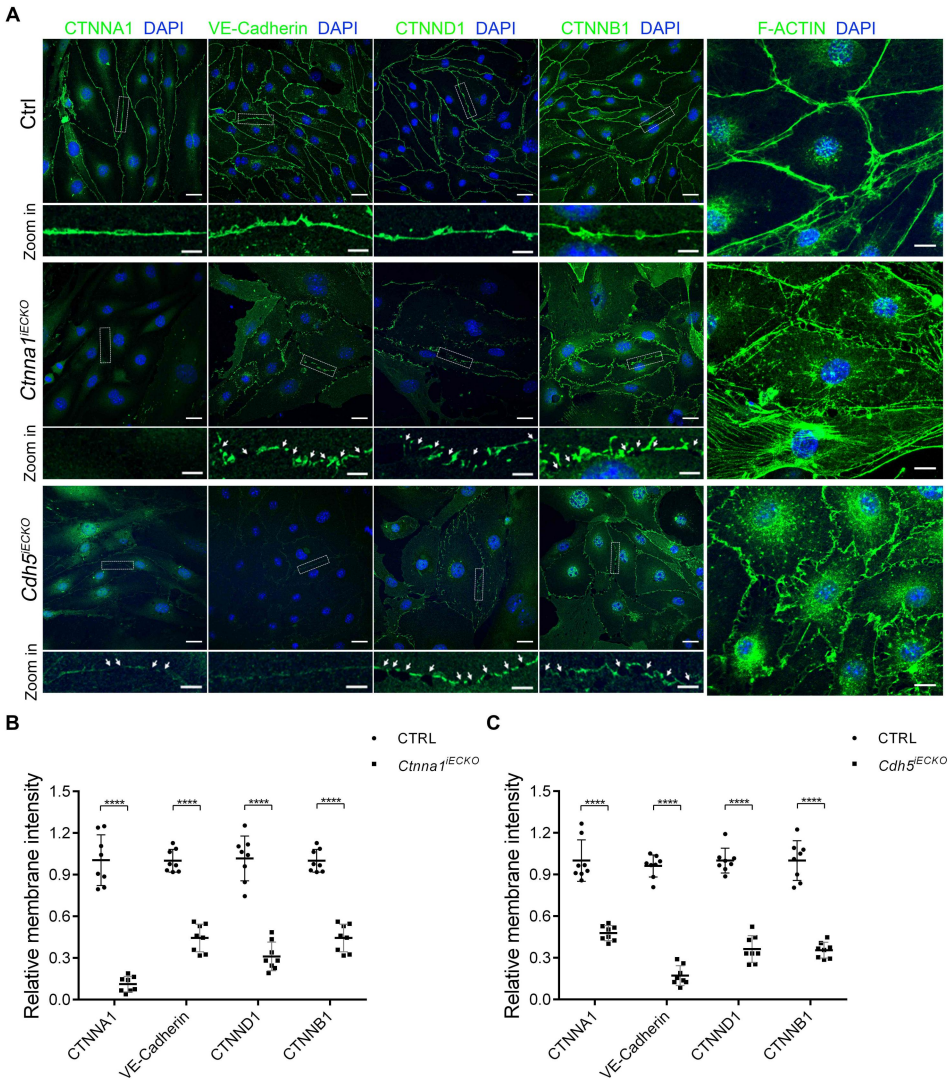

Figure S14. Disruption of adherens junctions and disorganization of F-ACTIN in isolated *Ctnna1*^{iECKO} and *Cdh5*^{iECKO} mouse lung endothelial cells. (A) Representative immunofluorescence images of isolated *Ctnna1*^{iECKO} and *Cdh5*$^{iECKO/iECKO}$ (hereafter named *Cdh5*^{iECKO}) mouse lung endothelial cells stained with anti-CTNNA1, VE-Cadherin, CTNND1, CTNNB1 or F-ACTIN antibody (green) and DAPI (blue). Dotted white boxes indicate magnified areas and white arrows point to discontinuous junctions. Scale bars, 25 μm and 5μm. (B and C) Quantification of relative membrane signal intensity of CTNNA1, VE-Cadherin, CTNND1 and CTNNB1 protein in isolated Ctrl, *Ctnna1*^{iECKO} and *Cdh5*^{iECKO} mouse lung endothelial

cells. Error bars, SD. *p*-values from multiple comparisons in two-way ANOVA with Sidak's multiple comparisons test (n=8), **** $p<0.0001$. Experiments were performed at least three times independently.

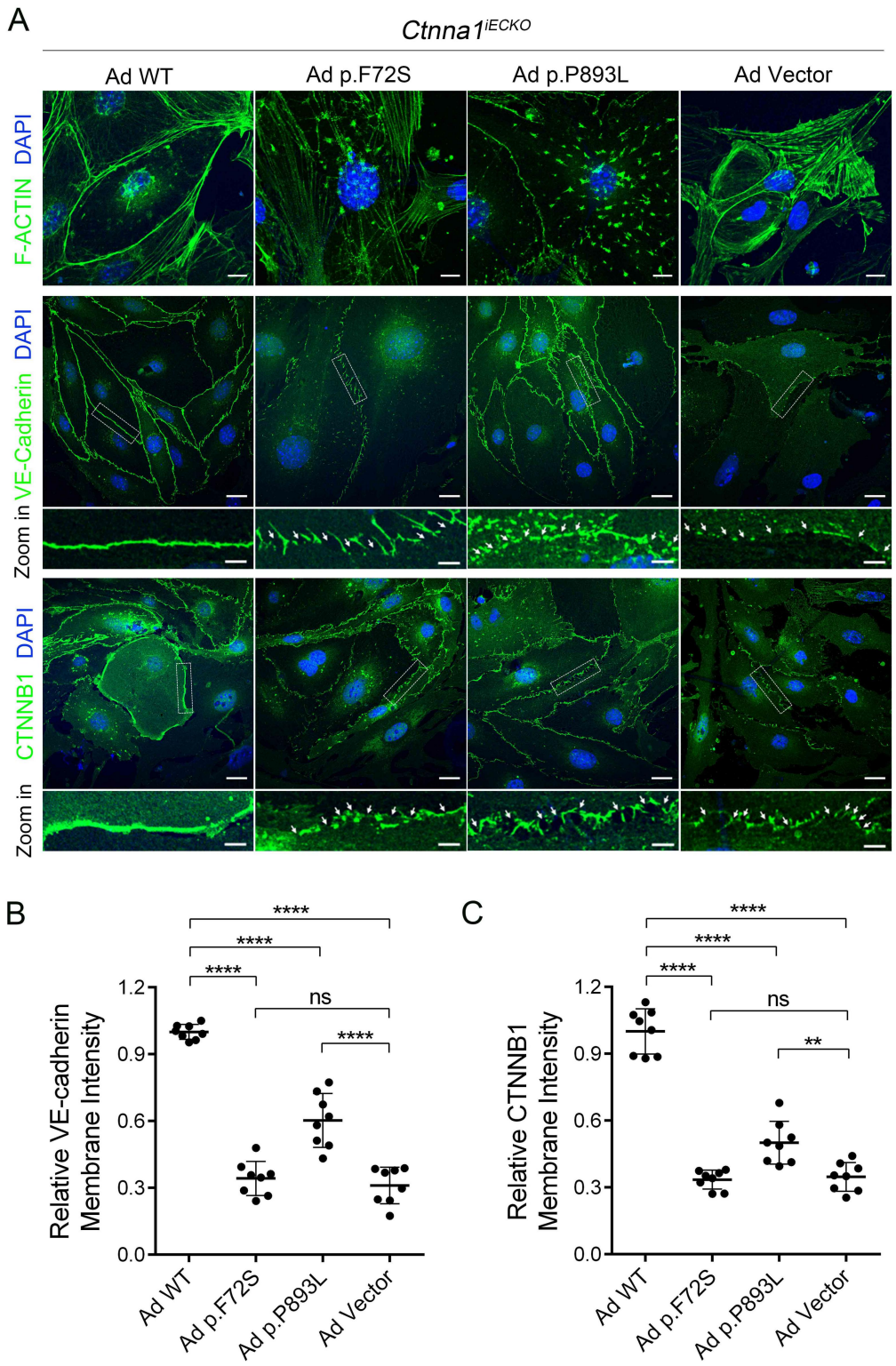

Figure S15. Overexpression of CTNNA1 mutant proteins in *Ctnna1*^{iECKO} mouse lung endothelial cells failed to rescue the disruption of adherens junction and disorganization of F-ACTIN. (A) Representative immunofluorescence images of isolated *Ctnna1*^{iECKO} mouse lung endothelial cells overexpressed with vector,

wildtype or mutant forms of *CTNNA1* co-stained with anti-CTNNA1, VE-Cadherin, CTNND1, CTNNB1 or F-ACTIN antibody (green) and DAPI (blue). Dotted white boxes indicate magnified areas and white arrows point to discontinuous junctions. Scale bars, 25 μm and 5μm. (B and C) Quantification of relative membrane signal intensity of CTNNA1, VE-Cadherin, CTNND1 and CTNNB1 protein in isolated *Ctnna1*^{iECKO} mouse lung endothelial cells overexpressed with vector, wildtype or mutant forms of *CTNNA1*. Error bars, SD. *p*-values from multiple comparisons in one-way ANOVA with Tukey's multiple comparisons test (n=8). ns, no significance; ** $p<0.01$, **** $p<0.0001$. Experiments were performed at least three times independently.

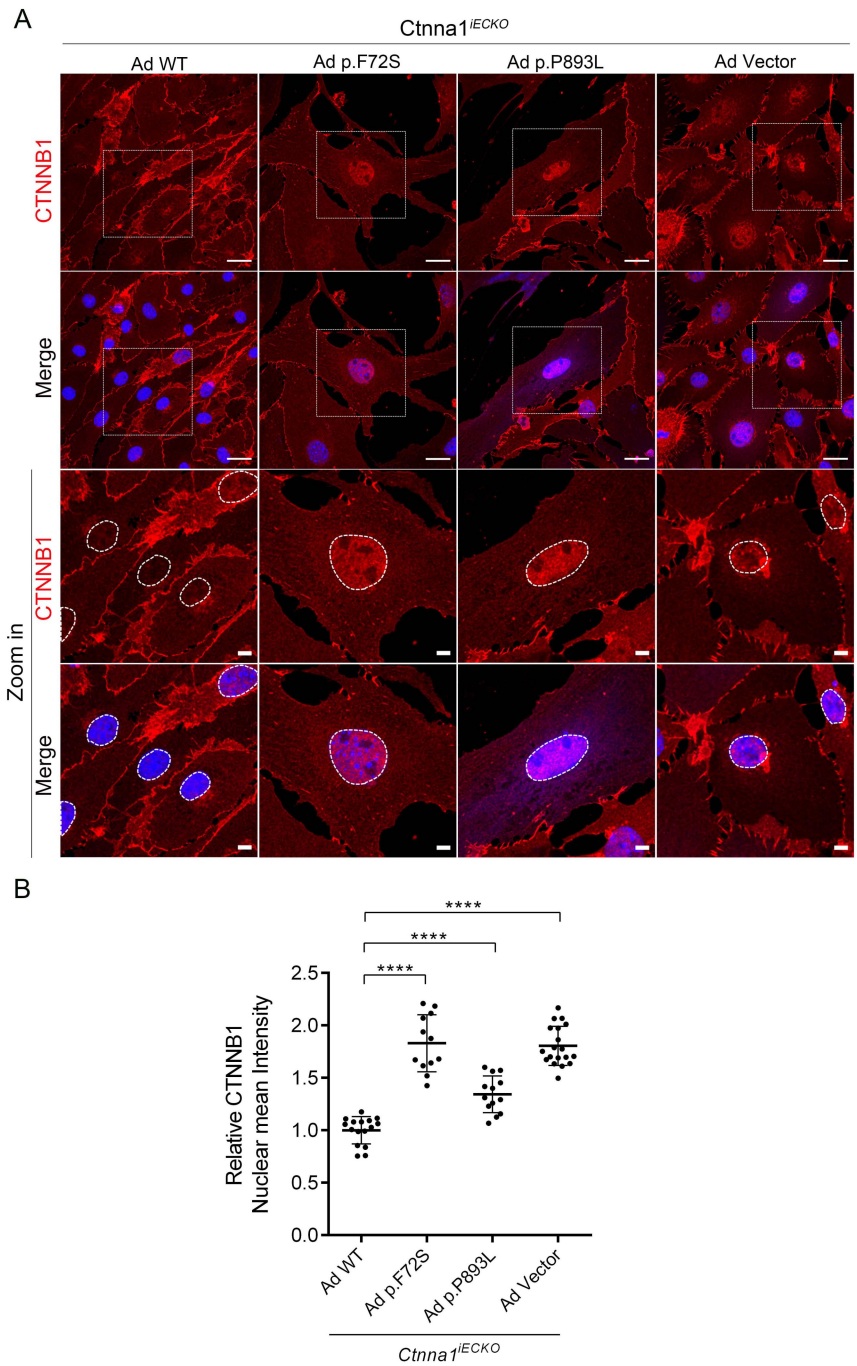

Figure S16. Overexpression of CTNNA1 mutant proteins in *Ctnna1^{iECKO}* mouse lung endothelial cells failed to inhibit β-catenin nuclear translocation. (A) Representative immunofluorescence images of isolated *Ctnna1^{iECKO}* mouse lung endothelial cells overexpressed with vector, wildtype or mutant forms of *CTNNA1* co-stained with anti- CTNNB1 antibody (red) and DAPI (blue). Dotted white boxes indicate magnified areas and dotted white circles indicate nucleus. Scale bars, 20 μm

1 and 5μm. (B and C) Quantification of relative nuclear mean intensity of CTNNB1

2 protein in isolated *Ctnna1*^{iECKO} mouse lung endothelial cells overexpressed with

3 vector, wildtype or mutant forms of *CTNNA1*. Error bars, SD. *p*-values from multiple

4 comparisons in one-way ANOVA with Dunnett's multiple comparisons test ($n \geq 8$).

5 **** $p<0.0001$. Experiments were performed at least three times independently.

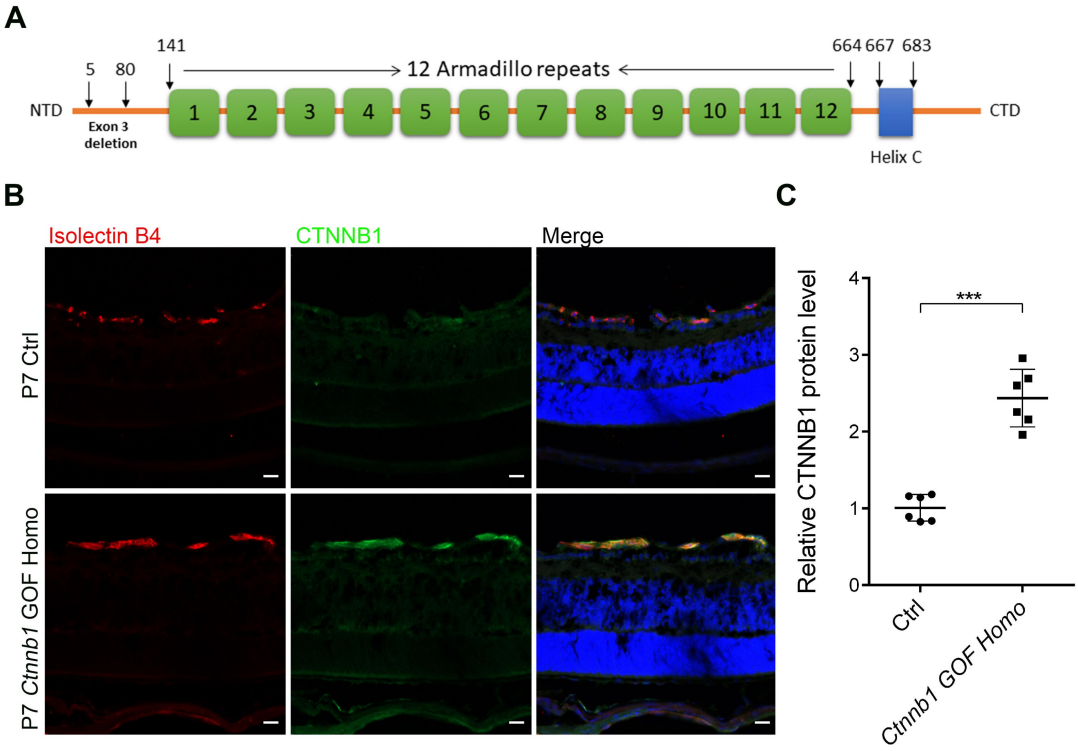

Figure S17. Deletion of exon3 of *Ctnnb1* in mouse ECs resulted in accumulation of CTNNB1 protein in retinal ECs. (A) Schematic representation of the CTNNB1 protein domains showing the location of exon 3 deleted in this study. (B) Anti-CTNNB1 (green) and IB4 (red) immunofluorescence of P7 Ctrl and *Ctnnb1* GOF Homo mice retinas. Scale bars, 20μm. (C) Quantification of relative CTNNB1 protein level. Error bars, SD. *p*-values, Student's t-test (sample size n=6 for both Ctrl and *Ctnnb1 GOF* Homo mice). ***p<0.001. Experiments were performed at least three times independently.

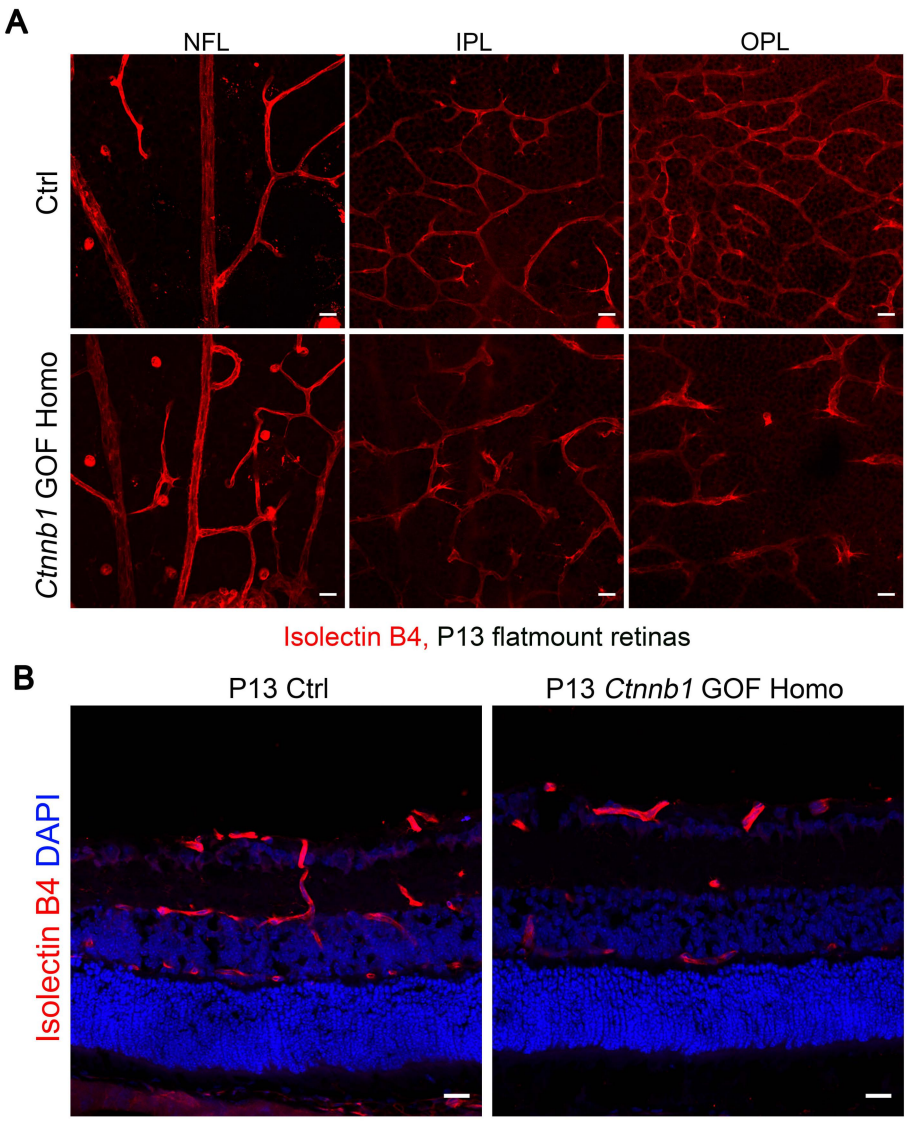

Figure S18. Gain of function of *Ctnnb1* allele in mice caused defect in deep vessel development. (A) Confocal projections of IB4 (red) stained NFL, IPL and OPL of P13 control and *Ctnnb1 GOF Homo* mice retina flat mounts. Scale bars, 20μm. (B) Retinal frozen sections of P13 Ctrl and *Ctnnb1 GOF Homo* mice co-stained with IB4 (red) and DAPI (blue). Scale bars, 20μm. Experiments were performed at least three times independently.

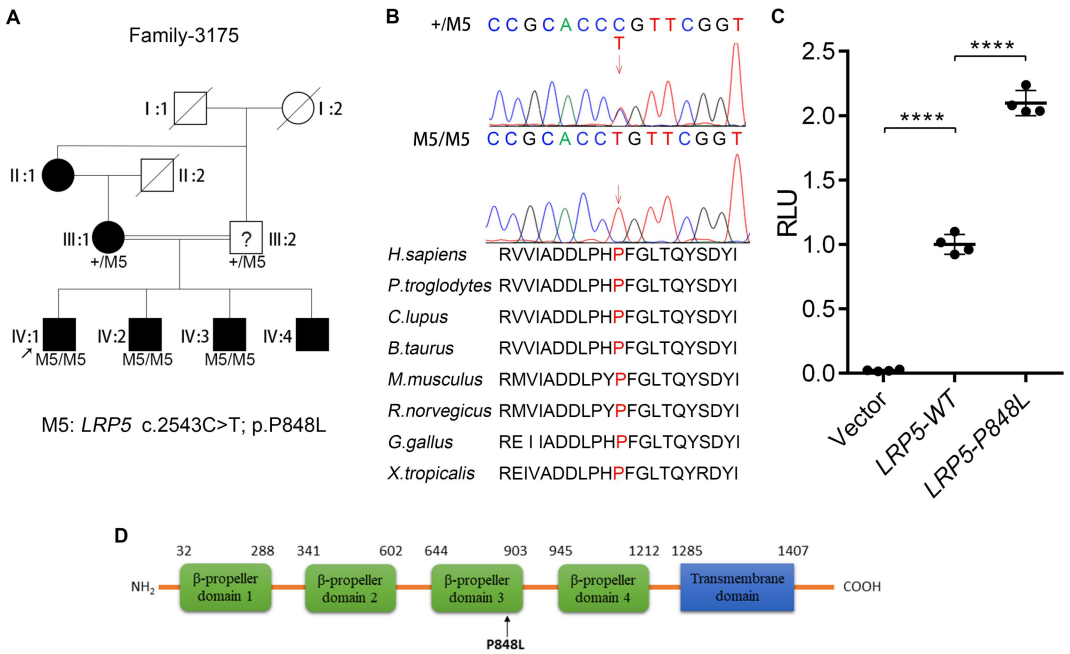

Figure S19. An *LRP5* mutation in an Indian family with FEVR. (A) FEVR pedigree map of an India FEVR family 3175. Black arrows indicate the proband (Affected patients are denoted in black). (B) Sanger sequencing analysis of family 3175 showing inheritance of FEVR. Red arrows indicate the changed nucleotides. Affected amino acids are denoted in red and are conserved among different species. (C) Results of luciferase reporter assay in HEK293 STF cells. Cells were transfected with plasmids containing *LRP5* (WT or p.P848L) or an empty vector (pCDNA3.1). Plasmids were co-transfected with *FZD4, NDP* and *Renillareniformis* (PGL4.1). The activity of WT protein was normalized as 1. Error bars, SD. *p*-values from multiple comparisons in one-way ANOVA with Dunnett's multiple comparisons test (Biological replicates n=4 for each group); **** $p<0.0001$. A representative result of three independent experiments was shown. (D) Schematic representation of the LRP5 protein domains showing the location of variants identified in this study. Experiments were performed at least three times independently.

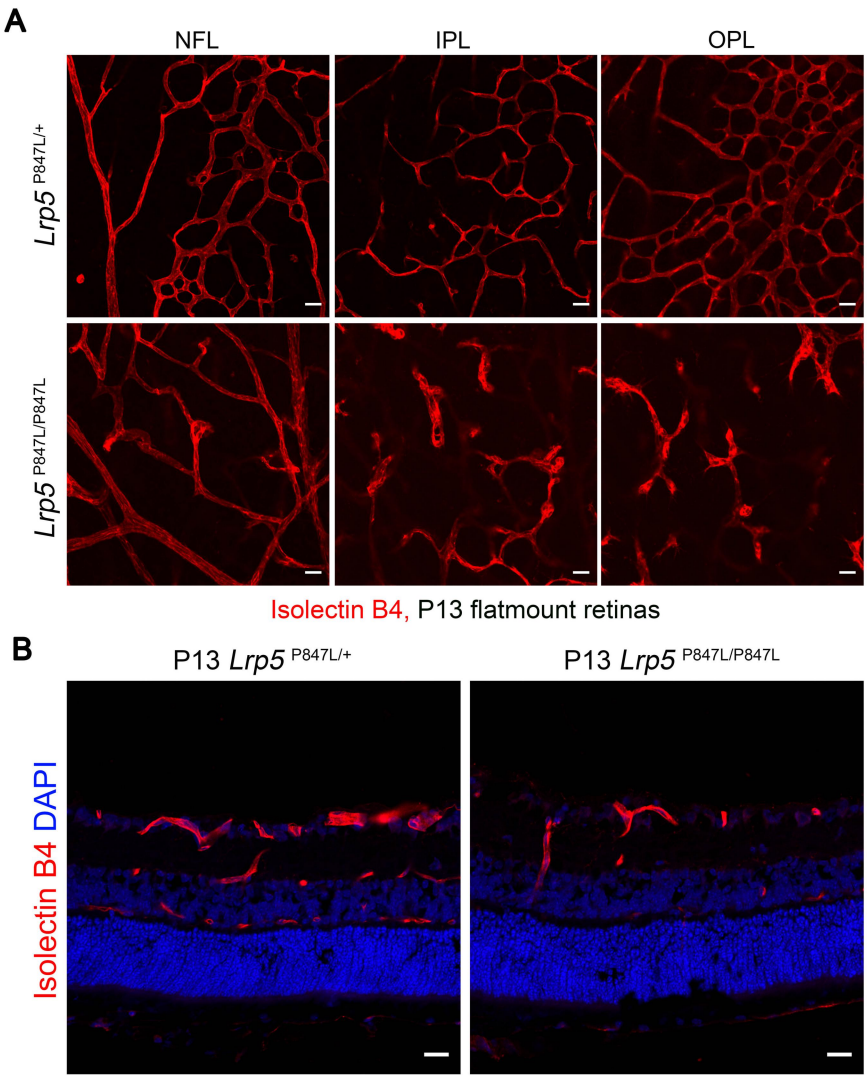

Figure S20. Mutation of *Lrp5 P847L* in mice caused delayed deep vessel development. (A) Confocal projections of IB4 (red) stained NFL, IPL and OPL of P13 control and *Lrp5*$^{P847L/P847L}$ mice retina flat mounts. Scale bars, 20μm. (B) Retinal frozen sections of P13 Ctrl and *Lrp5*$^{P847L/P847L}$ mice co-stained with IB4 (red) and DAPI (blue). Scale bars, 20μm. Experiments were performed at least three times independently.

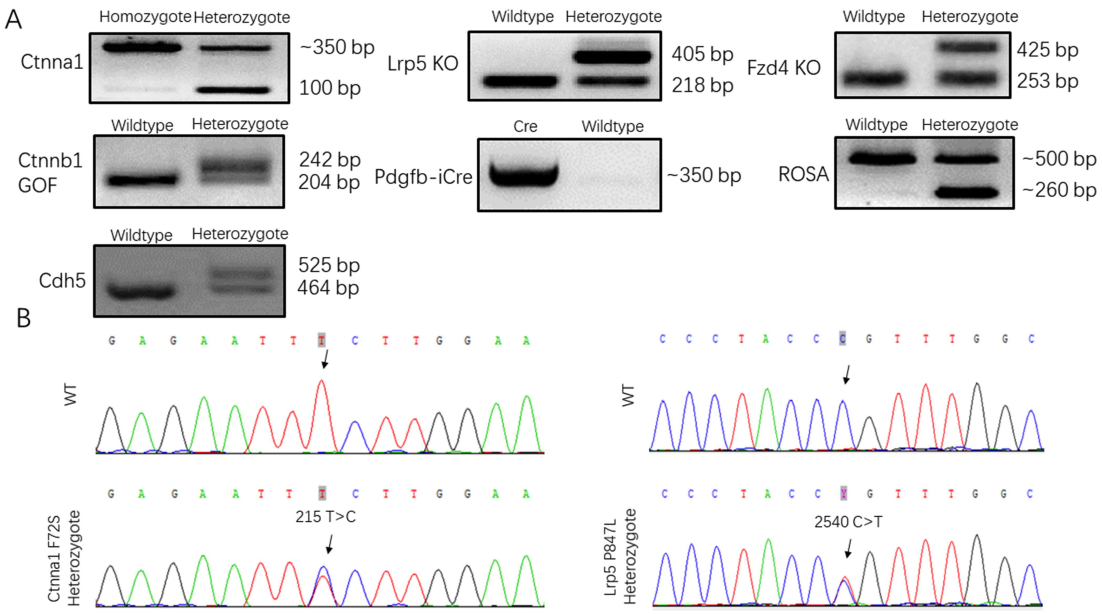

Figure S21. Genotyping of mouse models used in this study. (A) EtBr stained agarose gel for the identification of *Ctnna1, Cdh5, Lrp5, Fzd4, Ctnnb1 GOF, Pdgfb-iCre* and *ROSA* mice models. (B) Sanger sequencing analysis for the identification of *Ctnna1* F72S and *Lrp5* P847L mice.

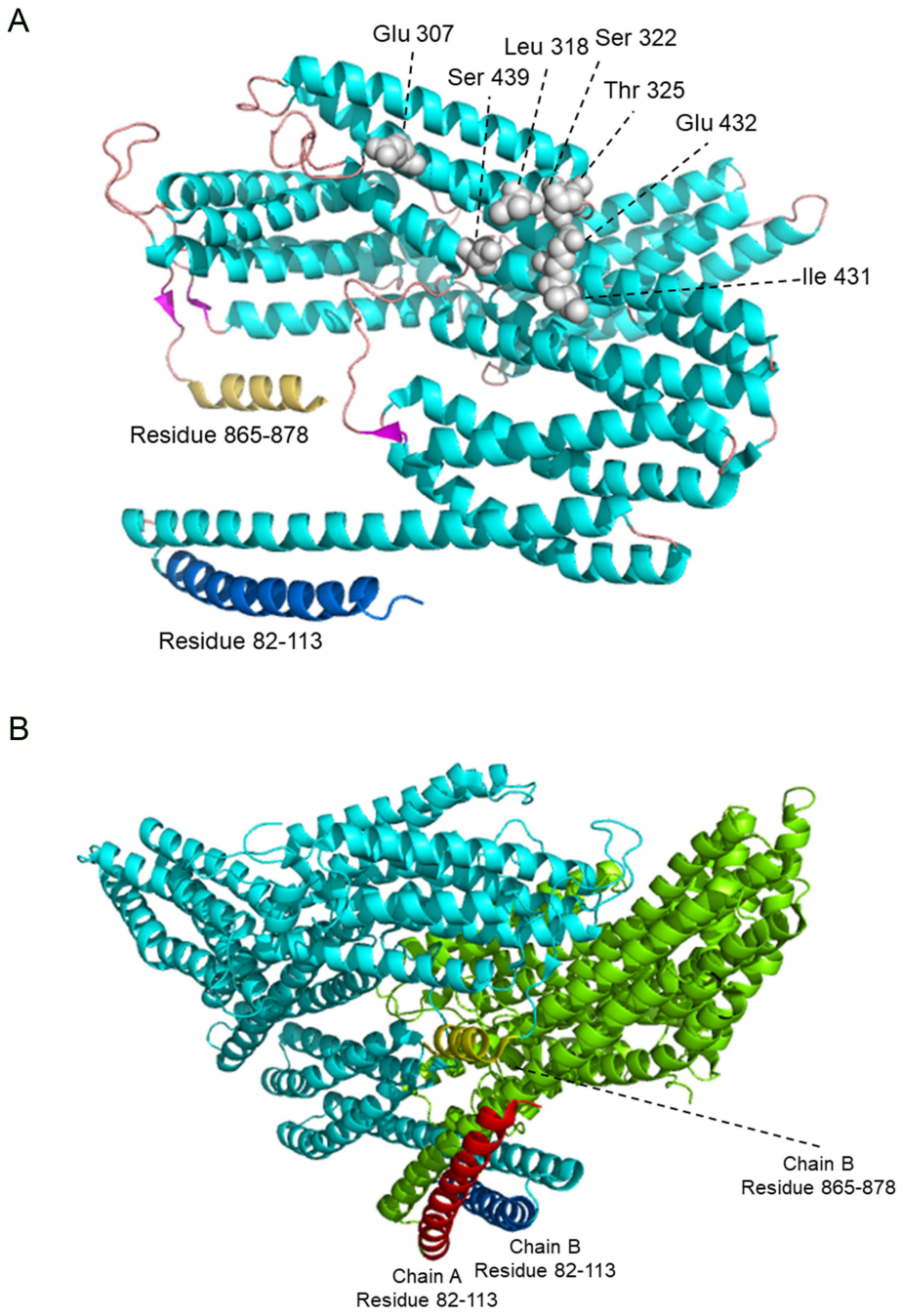

Figure S22. Crystal structure of human CTNNA1 (Protein Data Bank, PDB: 4IGG). (A) Polypeptide chain B of 4IGG (residues 82-878) structure model, helix, sheet and loop are shown as cartoon in cyan, magenta and orange, respectively. Blue and yellow cartoons represent N-terminal (residues 82-113) and C-terminal (residues 865-878) helix bundles. Gray spheres indicate residues altered by *CTNNA1* mutations that cause macular dystrophy. (B) Dimeric full-lenth structure of CTNNA1,

Polypeptide chain A (residues 82-861) and chain B (residues 82-878) are shown as cartoon in green and cyan. Red cartoon represents N-terminal helix of chain A. Blue and yellow cartoons represent N-terminal and C-terminal helix bundles of chain B.

1 Table S2. Clinical information of pedigree members in three families.

Pedigree members	Gender	Age at last exam.	Age at onset	Best Visual Acuity		Main Phenotype
				OD	OS	
Family-3016-Ⅱ:1	M	4 Y	NA	0.5[b]	NLP	OS, corneal opacity; OD, LIO
Family-3016-Ⅰ:1	M	31Y	NA	NA	NA	absence of peripheral vessels
Family-34-Ⅱ:1	F	16 M	at birth	NA	NA	OS, ILO, white hyperplasia[b]; OD, Sickle RD
Family-34-Ⅰ:2	F	25 Y	NA	NA	NA	absence of peripheral vessels, moderate leakage
Family-3004-Ⅱ:1	F	27 Y	NA	NA	NA	OS/OD, Sickle RD
Family-3004-Ⅰ:2	F	6 M	at birth	NA	NA	moderate leakage, abnormal anastomosis of peripheral vessels

2 Exam., examination; NA, not available; OD, right eye; OS, left eye; RD, retinal detachment; NLP, no light perception; LIO, Laser indirect Ophthalmoscope;

3 b, postoperative vision

4

1 Table S3. Pathogenicity programs applied to mutations in *CTNNA1*.

Location	Nucleotide change	Amino acid change	Number of cases	Allele frequency (%) in EVS	phyloP100way_ vertebrate	Polyphen	SIFT	CADD_phred
Exon3	c.215T>C	p. (Phe72Ser)	2	0	8.017	0.961 (probably damaging)	Deleterious (SIFT score=0.001)	29.1
Exon18	c.2678C>T	p. (Pro893Leu)	2	0	6.111	0.992 (probably damaging)	Deleterious (SIFT score=0.002)	33

2

3

4

5

6

7

1

1 **Table S4. *Ctnna1*$^{flox/+}$, *Tie2-Cre* intercross F2 genotype**

	+/ flox	flox/flox	+/flox, Tg	flox/flox,Tg
Quantity of offspring at P0	18	17	15	0
Percentage (%)	36	34	30	0
Expected mendelian ratio (%)	25	25	25	25

2

3 F1 genotype: Female: flox/flox; Male: +/flox, *Tie2-Cre.* Tg: *Tie2-Cre*.

4

1 **Table S5. Survival time of *Ctnna1*$^{iECKO/iECKO}$ mice tamoxifen induced from P1**

	Ctnna1$^{iECKO/iECKO}$
7 days (P8)	6
8 days (P9)	38
9 days (P10)	2
Total	46

2
3

1 **Table S6. Survival time of *Ctnna1*$^{iECKO/iECKO}$ mice tamoxifen induced from P6**

	Ctnna1$^{iECKO/iECKO}$
6 days (P12)	3
7 days (P13)	18
8 days (P14)	15
Total	36

2
3
4

1 **Table S7. *Ctnna1*$^{F72S/+}$ intercross F2 genotype**

	+/+	*F72S/+*	*F72S/F72S*
Quantity of offspring at P0	22	40	0
Percentage (%)	35.4%	64.5%	0
Expected mendelian ratio (%)	33.3%	66.7%	0

2

3 F1 genotype: Female: *Ctnna1*$^{F72S/+}$; Male: *Ctnna1*$^{F72S/+}$.

4

5

1 **Table S8. Primers for Sanger sequencing**

	Primers (5'-3')
CTNNA1 c.215T>C; p.F72S-F	AGTGGCAGTGTGATCTCCAG
CTNNA1 c.215T>C; p.F72S-R	ATGTCCCTCTGCAAGCATCT
CTNNA1 c.2678T>C; p.P893L-F	GCTTCTTACCACCCCTGTCT
CTNNA1 c.2678T>C; p.P893L-R	TTCAGTCTGCCCATTTCCCT
CTNNA1 c.1125-1131-delCAGGGAC; p. R376Cfs*27-F	GTGTACCCTGTTCTTGCTGC
CTNNA1 c.1125-1131delCAGGGAC; p. R376Cfs*27-R	ACTCAGAAAATTCAGCACCTCA
LRP5 c.2543C>T; p.P848L-F	GGGATCTTGCTGGTTTTCCAA
LRP5 c.2543C>T; p.P848L-R	GGGTCCAGGGTGTAGTGTGA

2

3 *CTNNA1* accession number: NM_001903

4 *LRP5* accession number: NM_002335

5

6

1 **Table S9 Primers for mouse genotyping**

Primer name	Primers (5'-3')
Ctnna1^{flox}-F	CATTTCTGTCACCCCCAAAGACAC
Ctnna1^{flox}-R	GCAAAATGATCCAGCGTCCTGGG
Cdh5^{flox}-F	GTCTCCTAGACTGGTTCCAAATGC
Cdh5^{flox}-R	CTTCTTCACCAGATCACTGCAA
Ctnnb1^{floxedExon}-F	CCTTCACGCAAGAGCAAGTAG
Ctnnb1^{floxedExon3}-R	ACCCTCTGAGCCCTAGTCAT
Pdgfb-iCre-ER-F	GCCGCCGGGATCACTCTCG
Pdgfb-iCre-ER-R	CCAGCCGCCGTCGCAACTC
Tie2-Cre-F	TGCCACGACCAAGTGACAGCAATG
Tie2-Cre-R	ACCAGAGACGCAAATCCATCGCTC
Rosa-tdt-F	CACTTGCTCTCCCAAAGTCG
Rosa-tdt-R	TAGTCTAACTCGCGACACTG
Rosa-tdt-KI	GTTATGTAACGCGGAACTCC
Ctnna1-p. F72S-F	GTGTCTGTCACCTAACTTACT
Ctnna1-p. F72S-R	CAGTTGTCTTCTGACTTCCA
Fzd4-10542	TGGAAAGGCTAATGGTCAAGATCGG
Fzd4-10543	AGAATTCACCAATCGGTTAGAACAC
Fzd4-10544	TGTCTGCTAGATCAGCCTCTGCCG
Fzd4-oIMR8960	CATCAACATTAAATGTGAGCGAGT
Lrp5-p. P847L-F	ATCATCATGGGCCAGCTGAG

Lrp5-p. P847L-R	TGGAAGAATCTCAGCCACAGT
LRP5-moIMR0632	CACTGCATGGATGCCAGTGAGGTGG
LRP5-moIMR0633	GCTGCCACTCATGGAGCCTTTATGC
LRP5-moIMR0634	CGCTACCGGTGGATGTGGAATGTGT

1
2

3

1 **Table S10. Antibodies for Immunohistochemistry**

Antibodies	Dilution ratio; Catalog #; Brand
Isolectin GS-IB4 Alexa Fluor™ 594 Conjugate	1:100 dilution; I21413; Invitrogen
Isolectin GS-IB4 Alexa Fluor™ 488 Conjugate	1:100 dilution; I21411; Invitrogen
Monoclonal ANTI-FLAG® M2 antibody produced in mouse	1:100 dilution; F3165; Sigma-Aldrich
rat anti-mouse Ter-119	1:20 dilution; 553670; BD Bioscience
anti-CLDN5 Alexa Fluor 488 conjugate	1:100 dilution; 352588; Thermo Fisher Scientific
rabbit anti-VE-Cadherin	1:1000 dilution; 2500; Cell Signaling Technology
rat anti-mouse VE-Cadherin	1:100 dilution; 555289; BD Bioscience
goat anti-mouse Esm-1	1:100 dilution; AF1999; R&D Systems
rabbit anti-GFAP	1:100 dilution; 12389; Cell Signaling Technology
goat anti-mouse Vegf164	1:100 dilution; AF-493-NA; R&D Systems
hamster anti-mouse DLL4	1:100 dilution; 130802; Biolegend
mouse anti-alpha catenin	1:100 dilution; 13-9700; Thermo Fisher Scientific
rabbit anti-alpha catenin	1:100 dilution; C2081; Sigma-Aldrich

rabbit anti-CTNNB1	1:1000 dilution; 9582; Cell Signaling Technology
rabbit anti-CTNND1	1:1000 dilution; 59854; Cell Signaling Technology
DAPI	1:1000 dilution; 4083; Cell Signaling Technology
Texas Red™-X Phalloidin	1:100 dilution; T7471; Thermo Fisher Sientific
goat anti-mouse IgG (H+L) Secondary Antibody, Alexa Fluor Plus 488	1:500 dilution; A32723; Invitrogen
goat anti-rat IgG (H+L) Secondary Antibody, Alexa Fluor™-488	1:500 dilution; A-11006; Invitrogen
donkey anti-goat IgG (H+L) Secondary Antibody, Alexa Fluor™-488	1:500 dilution; A32814; Invitrogen
goat anti-rabbit IgG (H+L) Secondary Antibody, Alexa Fluor™-488	1:500 dilution; A32721; Invitrogen
goat anti-rabbit IgG (H+L) Secondary Antibody, Alexa Fluor™-594	1:500 dilution; A32740; Invitrogen
goat anti-hamster IgG (H+L) Secondary Antibody, Alexa Fluor™-647	1:500 dilution; A-21451; Invitrogen

1 **Table S11. Primers for QPCR**

Primer name	Primers (5'-3')
Human-GAPDH-F	CTCTGCTCCTCCTGTTCGAC
Human-GAPDH-R	TTAAAAGCAGCCCTGGTGAC
Human-CTNNA1- F	GCGAATTGTGGCAGAGTGTA
Human-CTNNA1- R	GCAAGTCCCTGGTCTTCTTG
Human-CTNND1- F	ATGGGCTATGATGACCTGGA
Human-CTNND1- R	CAGCTCTGGCTGTCTCCAAT
Human-CDH5- F	GCTGGTCACTCTGCAAGACA
Human-CDH5- R	TCATCTGGGTCCTCAACAAA
Human-CLDN5- F	AAAGAGATCCCCCTGCATTT
Human-CLDN5- R	GTGAGCATCTCCTCCGAGAC
Human-OCLN- F	GCCCTCTGCAACCAATTTTA
Human-OCLN- R	TTCGAGTTTTCACAGCAAAGAA
Human-CCND1- F	TGAGGCGGTAGTAGGACAGG
Human-CCND1- R	GACCTTCGTTGCCCTCTGT
Human-MYC- F	CACCGAGTCGTAGTCGAGGT
Human-MYC- R	TTTCGGGTAGTGGAAAACCA
Human-CTNNB1- F	GTGGACCACAAGCAGAGTGC
Human-CTNNB1- R	TAGTTGCAGCATCTGAAAGATTCC

2
3

1 **Table S12. Antibodies for Western blots**

Antibodies	Dilution ratio; Catalog #; Brand
Monoclonal ANTI-FLAG® M2 antibody produced in mouse	1:100 dilution; F3165; Sigma-Aldrich
rabbit anti-VE-Cadherin	1:1000 dilution; 2500; Cell Signaling Technology
rabbit anti-CTNNB1	1:1000 dilution; 9582; Cell Signaling Technology
rabbit anti-CTNND1	1:1000 dilution; 59854; Cell Signaling Technology
anti-mouse IgG, HRP-linked Antibody	1:10000 dilution; 7076; Cell Signaling Technology
anti-rabbit IgG, HRP-linked Antibody	1:10000 dilution; 7074; Cell Signaling Technology

2

3

References:

1. Criswick VG, and Schepens CL. Familial exudative vitreoretinopathy. *American journal of ophthalmology.* 1969;68(4):578-94.
2. Collin RW, Nikopoulos K, Dona M, Gilissen C, Hoischen A, Boonstra FN, et al. ZNF408 is mutated in familial exudative vitreoretinopathy and is crucial for the development of zebrafish retinal vasculature. *Proceedings of the National Academy of Sciences of the United States of America.* 2013;110(24):9856-61.
3. Huang L, Zhang H, Cheng CY, Wen F, Tam PO, Zhao P, et al. A missense variant in FGD6 confers increased risk of polypoidal choroidal vasculopathy. *Nature genetics.* 2016;48(6):640-7.
4. Wang Y, Song F, Zhu J, Zhang S, Yang Y, Chen T, et al. GSA: Genome Sequence Archive<sup/>. *Genomics Proteomics Bioinformatics.* 2017;15(1):14-8.
5. National Genomics Data Center M, and Partners. Database Resources of the National Genomics Data Center in 2020. *Nucleic Acids Res.* 2020;48(D1):D24-D33.
6. Pitulescu ME, Schmidt I, Benedito R, and Adams RH. Inducible gene targeting in the neonatal vasculature and analysis of retinal angiogenesis in mice. *Nature protocols.* 2010;5(9):1518-34.
7. Junge HJ, Yang S, Burton JB, Paes K, Shu X, French DM, et al. TSPAN12 regulates retinal vascular development by promoting Norrin- but not Wnt-induced FZD4/beta-catenin signaling. *Cell.* 2009;139(2):299-311.
8. Wang J, Niu N, Xu S, and Jin ZG. A simple protocol for isolating mouse lung endothelial cells. *Sci Rep.* 2019;9(1):1458.
9. Xu Q, Wang Y, Dabdoub A, Smallwood PM, Williams J, Woods C, et al. Vascular Development in the Retina and Inner Ear : Control by Norrin and Frizzled-4, a High-Affinity Ligand-Receptor Pair. *Cell.* 2004;116(6):883-95.
10. Li VS, Ng SS, Boersema PJ, Low TY, Karthaus WR, Gerlach JP, et al. Wnt signaling through inhibition of beta-catenin degradation in an intact Axin1 complex. *Cell.* 2012;149(6):1245-56.
11. Zudaire E, Gambardella L, Kurcz C, and Vermeren S. A computational tool for quantitative analysis of vascular networks. *PLoS One.* 2011;6(11):e27385.